Atmos. Chem. Phys. Discuss., 15, 20449–20520, 2015
www.atmos-chem-phys-discuss.net/15/20449/2015/
doi:10.5194/acpd-15-20449-2015

Atmospheric Chemistry and Physics Discussions

The impact of residential combustion emissions on atmospheric aerosol, human health and climate

E. W. Butt[1], A. Rap[1], A. Schmidt[1], C. E. Scott[1], K. J. Pringle[1], C. L. Reddington[1], N. A. D. Richards[1], M. T. Woodhouse[1,2], J. Ramirez-Villegas[1,3], H. Yang[1], V. Vakkari[4], E. A. Stone[5], M. Rupakheti[6], P. S. Praveen[7], P. G. van Zyl[8], J. P. Beukes[8], M. Josipovic[8], E. J. S. Mitchell[9], S. M. Sallu[10], P. M. Forster[1], and D. V. Spracklen[1]

[1]Institute for Climate and Atmospheric Science, School of Earth and Environment, University of Leeds, Leeds, UK
[2]CSIRO Oceans and Atmosphere, Aspendale, Victoria, Australia
[3]International Centre for Tropical Agriculture, Cali, Colombia
[4]Finnish Meteorological Institute, Helsinki, Finland
[5]Department of Chemistry, University of Iowa, Iowa City, Iowa 52242, USA
[6]Institute for Advanced Sustainability Studies, Potsdam, Germany
[7]International Centre for Integrated Mountain Development, Kathmandu, Nepal
[8]North-West University, Unit for Environmental Sciences and Management, 2520 Potchefstroom, South Africa

[9]Energy Research Institute, School of Chemical and Process Engineering, University of Leeds, Leeds, UK
[10]Sustainability Research Institute, School of Earth and Environment, University of Leeds, Leeds, UK

Received: 29 May 2015 – Accepted: 24 June 2015 – Published: 29 July 2015

Correspondence to: E. W. Butt (e.butt@leeds.ac.uk)

Published by Copernicus Publications on behalf of the European Geosciences Union.

ACPD
15, 20449–20520, 2015

Abstract

Combustion of fuels in the residential sector for cooking and heating, results in the emission of aerosol and aerosol precursors impacting air quality, human health and climate. Residential emissions are dominated by the combustion of solid fuels. We use a global aerosol microphysics model to simulate the uncertainties in the impact of residential fuel combustion on atmospheric aerosol. The model underestimates black carbon (BC) and organic carbon (OC) mass concentrations observed over Asia, Eastern Europe and Africa, with better prediction when carbonaceous emissions from the residential sector are doubled. Observed seasonal variability of BC and OC concentrations are better simulated when residential emissions include a seasonal cycle. The largest contributions of residential emissions to annual surface mean particulate matter ($PM_{2.5}$) concentrations are simulated for East Asia, South Asia and Eastern Europe. We use a concentration response function to estimate the health impact due to long-term exposure to ambient $PM_{2.5}$ from residential emissions. We estimate global annual excess adult (> 30 years of age) premature mortality of 308 000 (113 300–497 000, 5th to 95th percentile uncertainty range) for monthly varying residential emissions and 517 000 (192 000–827 000) when residential carbonaceous emissions are doubled. Mortality due to residential emissions is greatest in Asia, with China and India accounting for 50 % of simulated global excess mortality. Using an offline radiative transfer model we estimate that residential emissions exert a global annual mean direct radiative effect of between −66 and +21 $mW\,m^{-2}$, with sensitivity to the residential emission flux and the assumed ratio of BC, OC and SO_2 emissions. Residential emissions exert a global annual mean first aerosol indirect effect of between −52 and −16 $mW\,m^{-2}$, which is sensitive to the assumed size distribution of carbonaceous emissions. Overall, our results demonstrate that reducing residential combustion emissions would have substantial benefits for human health through reductions in ambient $PM_{2.5}$ concentrations.

ACPD
15, 20449–20520, 2015

1 Introduction

Combustion of fuels within the home for cooking and heating, known as residential fuel combustion, is an important source of aerosol emissions with impacts on air quality and climate (Ramanathan and Carmichael, 2008; Lim et al., 2012). In most regions, residential emissions are dominated by the combustion of residential solid fuels (RSFs, see Table 1 for list of acronyms used in the study) such as wood, charcoal, agricultural residue, animal waste, and coal. Nearly 3 billion people, mostly in the developing world, depend on the combustion of RSFs as their primary energy source (Bonjour et al., 2013). RSFs are usually burnt in simple stoves or open fires with low combustion efficiencies, resulting in substantial emissions of aerosol. It has been suggested that reducing RSF emissions would be a fast way to mitigate climate and improve air quality (UNEP, 2011), but the climate impacts of RSF emissions are uncertain (Bond et al., 2013). Whilst it is clear that RSF combustion has substantial adverse impacts on human health through poor indoor air quality, there have been few studies quantifying the impacts on outdoor air quality and human health. Here, we use a global aerosol microphysics model to estimate the impacts of residential fuel combustion on atmospheric aerosol, climate and human health.

Residential combustion emissions include black carbon (BC), particulate organic matter (POM), primary inorganic sulfate and gas-phase SO_2. Residential emissions contribute substantially to the global aerosol burden, accounting for 25 % of global energy related BC emissions (Bond et al., 2013). In China and India, residential emissions are even more important, accounting for 50–60 % of BC and 60–80 % of organic carbon (OC) emissions (Cao et al., 2006; Klimont et al., 2009; Lei et al., 2011). Residential emissions are dominated by emissions from RSFs in many regions, due to poor combustion efficiency of RSFs and extensive use across the developing world (Bond et al., 2013). In China, residential combustion of coal is important, whereas across other parts of Asia and Africa, residential combustion of biomass also known as biofuel is dominant (Bond et al., 2013).

ACPD
15, 20449–20520, 2015

Estimates of residential emissions are typically "bottom-up", combining information on fuel consumption rates with laboratory or field emission factors. Obtaining reliable estimates of residential fuel use is difficult because these fuels are often collected by consumers and are not centrally recorded (Bond et al., 2013). Emission factors are hugely variable, depending on the type, size and moisture content of fuel, as well as stove design, operation and combustion conditions (Roden et al., 2006, 2009; Li et al., 2009; Shen et al., 2010). As a result, uncertainty in residential emissions may be as large as a factor 2 or more (Bond et al., 2004). There is a range of evidence that residential emissions may be underestimated. Firstly, emission factors for RSF combustion derived from laboratory experiments are often less than those derived under ambient conditions (Roden et al., 2009). Secondly, models typically underestimate observed aerosol absorption optical depth, BC and OC over regions associated with large RSF emissions such as in South and East Asia (Park et al., 2005; Koch et al., 2009; Ganguly et al., 2009; Menon et al., 2010; Nair et al., 2012; Fu et al., 2012; Moorthy et al., 2013; Bond et al., 2013; Pan et al., 2014). A further complication is that residential emissions, particularly from residential heating, also exhibit seasonal variability (Aunan et al., 2009; Stohl et al., 2013), but this is rarely implemented within global modelling studies.

Atmospheric aerosols interact with the Earth's radiation budget directly through the scattering and absorption of solar radiation (direct radiative effect (DRE) or aerosol–radiation interactions (ari)), and indirectly by modifying the microphysical properties of clouds (aerosol indirect effect (AIE) or aerosol–cloud interactions (aci)) (Forster et al., 2007; Boucher et al., 2013). The interaction of aerosol with radiation and clouds depends on properties of the aerosol, including mass concentration, size distribution, chemical composition and mixing state (Boucher et al., 2013). BC is strongly absorbing at visible and infrared wavelengths, exerting a positive DRE. BC particles coated with a non-absorbing shell have greater absorption compared to a fresh BC core due to a lensing effect (Fuller et al., 1999; Jacobson, 2001). POM and sulfate, scatter radiation exerting a negative (cooling) DRE. More recent studies have shown that a fraction of

ACPD
15, 20449–20520, 2015

organic aerosol can absorb light (Kirchstetter et al., 2004; Chen and Bond, 2010; Arola et al., 2011), with the light absorbing fraction termed "brown carbon". The net DRE of residential combustion emissions is a complex combination of these warming and cooling effects.

Aerosol also impacts climate through altering the properties of clouds. The cloud albedo or first AIE is the radiative effect due to a change in cloud droplet number concentration (CDNC), assuming a fixed cloud water content. The change in CDNC is governed by the number concentration of aerosols that are able to act as cloud condensation nuclei (CCN), which is determined by aerosol size and chemical composition (Penner et al., 2001; Dusek et al., 2006). Modelling studies have shown the importance of carbonaceous combustion aerosols to global CCN concentrations (Pierce et al., 2007; Spracklen et al., 2011a) and modification of cloud properties (Bauer et al., 2010; Jacobson, 2010). However, there is considerable variability in the size of particles emitted by combustion sources including those from residential sources (Venkataraman and Rao, 2001; Shen et al., 2010; Pagels et al., 2013; Bond et al., 2006) that will impact simulated CCN concentrations (Pierce et al., 2007, 2009; Reddington et al., 2011; Spracklen et al., 2011a) and AIE (Bauer et al., 2010; Spracklen et al., 2011a). Aerosols can further alter cloud properties through the second aerosol indirect effect and through semi-direct effects (Koch and Del Genio, 2010).

The net radiative effect (RE) of residential emissions depends on the fuel and combustion process (Bond et al., 2013). Carbonaceous emissions from residential biofuel exhibit higher POM : BC mass ratios, compared to residential coal, which emits more BC and Sulfur (Bond et al., 2013). Aunan et al. (2009) found that despite large BC emissions over Asia, RSF combustion emissions exerted a small net negative DRE because of co-emitted scattering aerosols, but did not include aerosol cloud effects. Jacobson (2010) reported increased cloud cover and depth from biofuel aerosol and gases, but also found a net positive RE. In contrast, Bauer et al. (2010) found the negative AIE from residential biofuel combustion to be 3 times greater than the positive DRE, resulting in a negative net RE. Unger et al. (2010) used a mass-only aerosol model to

ACPD
15, 20449–20520, 2015

calculate a positive AIE due to the residential sector. The review of Bond et al. (2013) identified a net negative RE (DRE and AIE) for biofuel with large uncertainty but a slight net positive RE (with low certainty) from residential coal (Bond et al., 2013).

In addition to impacting climate, aerosol from residential fuel combustion degrades air quality with adverse implications for human health. Epidemiologic research has confirmed a strong link between exposure to particulate matter (PM) and adverse health effects, including premature mortality (Pope III and Dockery, 2006; Brook et al., 2010). Exposure to $PM_{2.5}$ (PM with an aerodynamic dry diameter of $< 2.5\,\mu m$) is thought to be particularly harmful to human health (Pope III and Dockery, 2006; Schlesinger et al., 2006). Household air pollution, mostly from RSF combustion (Smith et al., 2014) in low and middle income countries is estimated to cause 4.3 million deaths annually (WHO, 2014a) making it one of the leading risk factors for global disease burden (Lim et al., 2012). Global estimates of premature mortality attributable to ambient (outdoor) air pollution range from 0.8 million to 3.7 million deaths per year, most of which occur in Asia (Cohen et al., 2005; Anenberg et al., 2010; WHO, 2014b). Emission inventories highlight residential combustion as one of the most important contributors to ambient $PM_{2.5}$ accounting for 55 % in Europe (EEA, 2014) and 33 % in China (Lei et al., 2011). However, while previous studies have estimated the human health impacts from ambient air pollution due to fossil fuel combustion (Anenberg et al., 2010), open biomass burning (Johnston et al., 2012; Marlier et al., 2013) and wind-blown dust (Giannadaki et al., 2014), fewer studies have quantified the impact of residential combustion on ambient quality and human health. Lim et al. (2012) estimated that 16 % of the global burden of ambient $PM_{2.5}$ was due to RSF sources but did not estimate premature mortality. Another study concluded that ambient $PM_{2.5}$ from cooking was responsible for 370 000 deaths in 2010 (Chafe et al., 2014), but did not include residential heating emissions, which will cause additional adverse impacts on human health (Johnston et al., 2013; Allen et al., 2013; Chen et al., 2013b).

Here we use a global aerosol microphysics model to make an integrated assessment of the impact of residential emissions on atmospheric aerosol, radiative effect

ACPD
15, 20449–20520, 2015

and human health. We used a radiative transfer model to calculate the DRE and first AIE due to residential emissions. To improve our understanding of the health impacts associated with these emissions, we combined simulated $PM_{2.5}$ concentrations with concentration-response functions from the epidemiological literature to estimate excess premature mortality.

2 Methods

2.1 Model description

We used the GLOMAP global aerosol microphysics model (Spracklen et al., 2005a), which is an extension to the TOMCAT 3-D global chemical transport model (Chipperfield, 2006). We used the modal version of the model, GLOMAP-mode (Mann et al., 2010), where aerosol mass and number concentrations are carried in 7 log-normal size modes: four hydrophilic (nucleation, Aitken, accumulation and coarse), and three non-hydrophilic (Aitken, accumulation and coarse) modes. The model includes size-resolved aerosol processes including primary emissions, secondary particle formation, particle growth through coagulation, condensation and cloud-processing and removal by dry deposition, in-cloud and below cloud scavenging. The model treats particle formation from both binary homogenous nucleation (BHN) of H_2SO_4-H_2O (Kulmala et al., 1998) and an empirical mechanism to simulate nucleation within the model boundary layer or boundary layer nucleation (BLN). The formation rate of 1 nm clusters ($J1$) within the BL is proportional to the gas-phase H_2SO_4 concentration ($[H_2SO_4]$) to the power of one (Sihto et al., 2006; Kulmala et al., 2006) according to $J1 = A[H_2SO_4]$ where A is the nucleation rate coefficient of $2 \times 10^{-6} s^{-1}$ (Sihto et al., 2006). GLOMAP-mode simulates multi-component aerosol and treats the following components: sulfate, dust, BC, POM and sea-salt. Primary carbonaceous combustion particles (BC and POM) are emitted as a non-hydrophilic distribution (Aitken insoluble mode). Dust is emitted into the insoluble accumulation and coarse modes. Non-hydrophilic particles are trans-

ACPD
15, 20449–20520, 2015

ferred into hydrophilic particles through coagulation and condensation processes. The model uses a horizontal resolution of 2.8° by 2.8° and 31 vertical levels between the surface and 10 hPa. Large-scale transport and meteorology is specified at six hourly intervals from the European Centre for Medium-Range Weather Forecasts (ECMWF) analyses interpolated to model timestep. All model simulations are for the year 2000, completed after a 3 month model spin up. Concentrations of oxidants OH, O_3, H_2O_2, NO_3 and HO_2 are specified using six hourly monthly mean 3-D gridded concentrations from a TOMCAT simulation with detailed tropospheric chemistry (Arnold et al., 2005).

2.2 Emissions

The model uses gas phase SO_2 emissions for both continuous (Andres and Kasgnoc, 1998) and explosive (Halmer et al., 2002) volcanic eruptions. Open biomass burning emissions are from the Global Fire Emission Database (van der Werf et al., 2004). Oceanic dimethyl-sulphide (DMS) emissions are calculated using an ocean surface DMS concentration database (Kettle and Andreae, 2000) combined with a sea–air exchange parameterization (Nightingale et al., 2000). Emissions of sea salt were calculated using the scheme of Gong (2003). Biogenic emissions of terpenes are taken from the Global Emissions Inventory Activity database and are based on Guenther et al. (1995). Daily-varying dust emission fluxes are provided by AeroCom (Dentener et al., 2006).

Annual mean anthropogenic emissions of gas-phase SO_2 and carbonaceous aerosol for the year 2000 are taken from the Atmospheric Chemistry and Climate Model Intercomparison Project (ACCMIP) (Lamarque et al., 2010). This dataset includes emissions from energy production and distribution, industry, land transport, maritime transport, residential and commercial and agricultural waste burning on fields. To test the sensitivity to anthropogenic emissions, we completed sensitivity studies (see Sect. 2.6) using anthropogenic emissions from the MACCity (MACC/CityZEN projects) emission dataset for the year 2000 (Granier et al., 2011). MACCity emissions are derived from ACCMIP and apply a monthly varying seasonal cycle for anthropogenic emissions

ACPD
15, 20449–20520, 2015

(Granier et al., 2011). In both emissions datasets, anthropogenic carbonaceous emissions are based on the Speciated Particulate Emissions Wizard (SPEW) inventory (Bond et al., 2007). In GLOMAP, anthropogenic carbonaceous emissions are added to the lowest model layer, while open biomass burning emissions are emitted between the surface and 6 km (Dentener et al., 2006).

We isolate the impact of residential fuel combustion through simulations where we switch off emissions from the residential and commercial sector, which we refer to as the "residential" sector. Residential fuels used in small-scale combustion for cooking, heating, lighting and auxiliary engines, consist of many different types such as RSFs (biomass/biofuel and coal) and hydrocarbon-based fuels including kerosene and liquefied petroleum gas (LPG), gasoline and diesel. The ACCMIP and MACCity residential datasets do not allow us to isolate the impacts of different RSFs separately from other residential hydrocarbon-based fuels, but according to the results from the Greenhouse Gas and Air Pollution Interactions and Synergies (GAINS) model, typically $\geq 90\,\%$ of PM emissions can be attributed to RSFs within most regions, of which a large proportion is from biomass sources. Compared with residential hydrocarbon-based fuels, RSFs typically burn at lower combustion efficiencies resulting in substantially higher aerosol emissions (Venkataraman et al., 2005). Residential kerosene wick lamps can produce substantial emissions (Lam et al., 2012), however these are not included in the ACCMIP and MACCity datasets. Residential biofuel and coal emissions from ACCMIP and MACCity differ to previous global emission inventories (Bond et al., 2004, 2007) through the incorporation of updated emissions factors from field measurements (Roden et al., 2006, 2009; Johnson et al., 2008) and laboratory experiments for biofuel sources in India (Venkataraman et al., 2005; Parashar et al., 2005), and residential coal sources in China (Chen et al., 2005, 2006; Zhi et al., 2008). In both the ACCMIP and MACCity emission datasets, global emissions for the residential and commercial sectors are BC ($\sim 1.9\,\mathrm{Tg\,yr^{-1}}$), POM ($\sim 11.0\,\mathrm{Tg\,POM\,yr^{-1}}$) and SO_2 ($\sim 8.3\,\mathrm{Tg\,SO_2\,yr^{-1}}$).

Figure 1 shows the spatial distribution of BC, POM, and SO_2 emissions from the residential sectors in the ACCMIP dataset (Lamarque et al., 2010). Residential emissions

ACPD
15, 20449–20520, 2015

are greatest over densely populated regions of Africa and Asia where infrastructure and income do not allow access to clean sources of residential energy, with emissions dominated by RSF combustion. The dominant fuel type varies spatially resulting in distinct patterns in pollutant emission ratios (Fig. 1d–e). Residential emissions are dominated by biofuel (biomass) combustion in sub-Saharan Africa, South Asia and parts of Southeast Asia and characterised by low BC : POM and high BC:SO_2 ratios. Residential coal combustion is more important in parts of Eastern Europe, the Russian Federation and East Asia characterised by higher BC : POM and lower BC:SO_2 ratios. Regions showing the use of a combination fuels such as biofuel and coal are characterised by low BC : POM and low BC : SO_2 such as in Europe. In the ACCMIP and MACCity datasets, residential sources account for 38 % of global total anthropogenic BC but a larger proportion (61 %) of total global anthropogenic POM emissions. The regional contribution of residential emissions can be even greater (Fig. 1f). For China, residential emissions represent 40 % of anthropogenic BC and 60 % of anthropogenic POM of emissions. In India, residential emissions represent 63 % of anthropogenic BC and 78 % of anthropogenic OC emissions. Fractional residential POM emissions are also large for other regions including parts of Western Europe, Eastern Europe and the Russian Federation and sub-Saharan Africa.

We assume primary particles from combustion sources are emitted with a fixed log-normal size distribution with a specified geometric mean diameter (D) and standard deviation (σ). Assumptions regarding D and σ for each experiment are detailed in the footnotes of Table 3. This assumed initial size distribution assumption accounts for both the size of primary particles at the point of emission and the sub-grid scale dynamical processes that contribute to changes in particle size and number concentrations at short time scales after emission (Pierce and Adams, 2009; Reddington et al., 2011). Subsequent aging and growth of the particles are determined by microphysical processes such as coagulation, condensation and cloud processing simulated by the model. We assume that 2.5 % of SO_2 from anthropogenic and volcanic sources is emitted as primary sulfate particles.

ACPD
15, 20449–20520, 2015

2.3 In-situ measurements

To evaluate our model, we synthesised in-situ measurements of BC, OC and $PM_{2.5}$ concentrations, aerosol number size distribution and estimates of the contribution of biomass derived BC from ^{14}C analysis. GLOMAP has been evaluated for locations in North America (Mann et al., 2010; Spracklen et al., 2011a), the Arctic (Browse et al., 2012; Reddington et al., 2013) and Europe (Schmidt et al., 2011). Here, we focus our evaluation at locations that may be strongly influenced by residential emissions (Fig. 1) and where the model has not been previously evaluated. We focus on rural and background locations because these are more appropriate for comparison to global models with coarse spatial resolutions.

Figure 2 shows the locations of observations used in this study. Information on the measurements for each location is reported in Table 2. The technique and instruments used to measure BC and OC vary across the different sites (see Table 2). Thermal-optical techniques measure elemental carbon (EC) whereas optical techniques measure BC. Previous studies have documented systematic differences between these techniques, but concluded that measurement uncertainties are generally larger than the differences between the measurement techniques (Bond et al., 2004, 2007). We therefore treat different measurement techniques identically and consider EC and BC to be equivalent. For Eastern Europe, we used BC and OC mass concentrations from Czech Republic and Slovenia (Table 2). For South Africa, we used $PM_{2.5}$ and BC mass and aerosol number size distribution (Vakkari et al., 2013). For South Asia, we used BC mass from the Integrated Campaign for Aerosols gases and Radiation Budget (ICARB) field campaign at 8 locations across the Indian mainland and islands (Moorthy et al., 2013). For South Asia, we also used $PM_{2.5}$, EC and OC mass, and aerosol number size distribution from the island of Hanimaadhoo in the Maldives (Stone et al., 2007), and EC and OC measurements from Godavari in Nepal (Stone et al., 2010). For East Asia, we used EC and OC mass data compiled by Fu et al. (2012) for 2 background (Qu et al., 2008) and 7 rural sites (Zhang et al., 2008; Han et al., 2008) in China, while measure-

ACPD
15, 20449–20520, 2015

ments from Gosan, South Korea were taken from (Stone et al., 2011). Few long-term observations of CCN are available, so instead we use the number concentration of particles greater than 50 nm dry diameter (N_{50}) and 100 nm (N_{100}) as a proxy for CCN number concentrations. We calculated N_{50} and N_{100} concentrations from aerosol number size distribution measurements at Hanimaadhoo, Botsalano, Marikana and Welgegund (see Table 2). We note this approach does not account for the impact of particle composition on CCN activity.

We also use information on BC fossil and non-fossil fractions as obtained from three separate source apportionment studies (Gustafsson et al., 2009; Sheesley et al., 2012; Bosch et al., 2014) that use ^{14}C analysis of carbonaceous aerosol taken at Hanimaadhoo in the Indian Ocean. This technique determines the fossil and non-fossil fractions of carbonaceous aerosol, since ^{14}C is depleted in fossil fuel aerosol (half-life 5730 years), whereas non-fossil aerosol (e.g. biofuel, open biomass burning and biogenic emissions) shows a contemporary ^{14}C content.

2.4 Calculating health effects

We calculate annual excess premature mortality from exposure to ambient $PM_{2.5}$ using concentration response functions (CRFs) from the epidemiological literature that relate changes in $PM_{2.5}$ concentrations to the relative risk (RR) of disease. CRFs are uncertain and have been previously based on the relationship between RR and $PM_{2.5}$ concentrations using either a log-linear model (Ostro, 2004) or a linear model (Cohen et al., 2004). These CRFs were based on the American Cancer Society Prevention cohort study, where observed annual mean $PM_{2.5}$ concentrations were typically below 30 $\mu g\,m^{-3}$. The log-linear model was recommended by the WHO for use in ambient air pollution burden of disease estimates at the national level (Ostro, 2004) due to the concern that linear models would produce unrealistically large RR estimates when extrapolated to higher $PM_{2.5}$ concentrations above that of 30 $\mu g\,m^{-3}$. The log-linear models have been used in various modelling studies (Anenberg et al., 2010; Schmidt et al., 2011; Partanen et al., 2013). More recent models have been proposed to relate dis-

ACPD
15, 20449–20520, 2015

ease burden to different combustion sources in order to capture RR over a larger range of $PM_{2.5}$ concentrations up to 300 $\mu g\,m^{-3}$ (Burnett et al., 2014). However, given that we use a global model with relatively large spatial resolution where $PM_{2.5}$ concentrations very rarely exceed 100 $\mu g\,m^{-3}$, we employ the log-linear model of Ostro (2004). This model is also consistent with the RR estimates used for long-term documented $PM_{2.5}$ mortality (above cohort study), and the uncertainty in the function (represented by the 5th to 95th percentile ranges) will likely account for the uncertainty in our analysis. We calculate RR for cardiopulmonary diseases and lung cancer following Ostro (2004):

$$RR = \left[\frac{(PM_{2.5,\,control} + 1)}{(PM_{2.5,\,R\_off} + 1)}\right]^{\beta} \quad (1)$$

where $PM_{2.5,control}$ is annual mean simulated $PM_{2.5}$ concentrations of the control experiments and $PM_{2.5,R\_off}$ is a perturbed experiment where residential emissions have been removed. The cause-specific coefficient (β) is an empirical parameter with separate values for lung cancer (0.23218, 95 % confidence interval of 0.08563–0.37873) and cardiopulmonary diseases (0.15515, 95 % confidence interval of 0.05624–0.2541). To calculate the disease burden attributable to the RR, known as the attributable fraction (AF), we follow Ostro (2004):

$$AF = (RR - 1)/RR \quad (2)$$

To calculate the number of excess premature mortality in adults over 30 years of age, we apply AF to the total number of recorded deaths from the diseases of interest:

$$\Delta M = AF \times M_0 \times P_{30+} \quad (3)$$

where M_0 is the baseline mortality rate for each disease risk and P_{30+} is the exposed population over 30 years of age. We use country specific baseline mortality rates from the WHO Global Burden of Disease Updated 2004 (Mathers et al., 2008) for the year 2004, and human population data from the Gridded World Population (GWP; version3) project (SEDAC, 2004) for the year 2000.

ACPD
15, 20449–20520, 2015

2.5 Calculating radiative effects

We quantified the DRE and first AIE of residential emissions using an offline radiative transfer model (Edwards and Slingo, 1996). This model has nine bands in the longwave (LW) and six bands in the shortwave (SW). We use a monthly mean climatology of water vapour, temperature and ozone based on European Centre for Medium-Range Weather Forecasts reanalysis data, together with surface albedo and cloud fields from the International Satellite Cloud Climatology Project (ISCCP-D2) (Rossow and Schiffer, 1999) for the year 2000.

Following the methodology described in Rap et al. (2013) and Scott et al. (2014), we estimate the DRE using the radiative transfer model to calculate the difference in net (SW + LW) top-of-atmosphere (TOA) all-sky radiative flux between model simulations with and without residential emissions. A refractive index is calculated for each mode, as the volume-weighted mean of the refractive indices for the individual components (including water) present (given at 550 nm in Table A1 of Bellouin et al., 2011). Coefficients for absorption and scattering, and asymmetry parameters, are then obtained from look-up tables containing all realistic combinations of refractive index and Mie parameter (particle radius normalised to the wavelength of radiation), as described by Bellouin et al. (2013).

To determine the first AIE we calculate the contribution of residential emissions to cloud droplet number concentrations (CDNC). We calculate CDNC using the parameterisation of cloud drop formation (Nenes and Seinfeld, 2003; Fountoukis and Nenes, 2005; Barahona et al., 2010) as described by Pringle et al. (2009). The maximum supersaturation (SS_{max}) of an ascending cloud parcel depends on the competition between increasing water vapour saturation with decreasing pressure and temperature, and the loss of water vapour through condensation onto activated particles. Monthly mean aerosol size distributions are converted to a supersaturation distribution where the number of activated particles can be determined for the SS_{max}. CDNC are calculated using a constant up-draught velocity of 0.15 ms^{-1} over sea and 0.3 ms^{-1} over

ACPD
15, 20449–20520, 2015

land, which is consistent with observations for low-level stratus and stratocumulus clouds (Pringle et al., 2012). In reality, up-draught velocities vary, but the use of average velocities in previous GLOMAP studies has been shown to capture observed relationships between particle number and CDNC (Pringle et al., 2009), as well as reproducing realistic CDNC (Merikanto et al., 2010). The AIE is calculated using the methodology described previously (Spracklen et al., 2011a; Schmidt et al., 2012; Scott et al., 2014) where a control uniform cloud droplet effective radius r_{e1} = 10 µm is assumed to maintain consistency with the ISCCP determination of liquid water path. For each perturbation experiment the effective radius r_{e2} is calculated:

$$r_{e2} = r_{e1} \times \left(\mathrm{CDNC}_1/\mathrm{CDNC}_2\right)^{\frac{1}{2}} \quad (4)$$

where CDNC_1 represents a control simulation including residential emissions and CDNC_2 represents a simulation where residential emissions have been removed. The AIE is calculated by comparing the net TOA radiative fluxes using the different r_{e2} values derived for each perturbation experiment, to that of the control where r_{e1} is fixed. We do not calculate the cloud lifetime (second indirect effect), semi-direct effects or snow albedo changes. We also do not account for light absorbing brown carbon and the lensing effect of BC particles coated with a non-absorbing shell, and thus are unable to estimate the full climate impact of residential combustion emissions.

2.6 Model simulations

Table 3 reports the model experiments used in this study. These simulations explore uncertainty in residential emission flux and emitted carbonaceous aerosol size distributions and the impact of particle formation. We test two different emission data sets (see Sect. 2.2 for details) allowing us to explore the role of seasonally varying emissions compared to annual mean emissions. We refer to the simulation using the ACCMIP emissions (annual mean emissions) with the standard model setup as the baseline simulation (res_base), while all other simulations explore key uncertainties relative to

ACPD
15, 20449–20520, 2015

res_base or use the MACCity emission database of monthly varying anthropogenic emissions (res_monthly). To allow us to quantify the impact of residential emissions we conduct simulations where residential emissions (BC, OC and SO_2) have been switched off (re_base_off and res_monthly_off). To account for uncertainties in the nucleation scheme, we conduct simulations where only BHN is able to contribute to new particle formation (res_BHN and res_BHN_off), while all other simulations include both BHN and BLN. For the majority of our simulations, we use emitted particle size used by Stier et al. (2005). To account for the uncertainty in the size of emitted residential carbonaceous combustion aerosol (D) and uncertainty of sub-grid ageing of the size distribution, we conduct simulations spanning the range of observed size distributions for primary BC and OC residential combustion particles, while keeping emission mass fixed. We use AerCom recommended particle size settings (res_aero) (Dentener et al., 2006) and following a similar approach to Bauer et al. (2010), we use the range identified by Bond et al. (2006) for lower (res_small) and upper (res_large) estimates for D. To account for possible low biases in residential emission flux, we conduct simulations where residential primary carbonaceous combustion aerosol mass (BC and OC) are doubled relative to the baseline simulation (res_×2) and the simulation using monthly mean anthropogenic emissions (res_monthly_×2). We also perform experiments where only residential BC and OC emissions are doubled separately relative to Base (res_BC×2 and res_POM×2) to explore uncertainties in emission ratio. While the uncertainties in primary carbonaceous aerosol emissions are thought to be higher than for gas phase SO_2 (Klimont et al., 2009), we also conduct an experiment where we double residential SO_2 emissions (res_SO2×2).

ACPD
15, 20449–20520, 2015

3 Results

3.1 Model evaluation

Figure 3 compares observed and simulated monthly mean BC, OC and $PM_{2.5}$ concentrations, and normalised mean bias factor (NMBF) (Yu et al., 2006). The baseline simulation underestimates observed BC (NMBF = −2.33), OC (NMBF = −5.02) and $PM_{2.5}$ (NMBF = −1.33) concentrations. The greatest model underprediction is across East Asia (BC: NMBF = −2.61, OC: NMBF = −6.56 and $PM_{2.5}$: NMBF = −1.94). Over South Asia the model is relatively unbiased against OC (NMBF = 0.41) but underestimates BC (NMBF = −2.54). In contrast, over Europe the model is unbiased against BC (NMBF = 0.01) but underestimates OC (NMBF = −2.63). The simulation with monthly varying emissions compares slightly better with observations compared to the baseline simulation, but still underestimates BC (NMBF = −2.29), OC (NMBF = −4.92) and $PM_{2.5}$ (NMBF = −1.34), suggesting that seasonality in emissions has little impact on reducing model bias. The low bias in our model, particularly for BC and OC is consistent with previous modelling studies using bottom-up emission inventories in South Asia (Ganguly et al., 2009; Menon et al., 2010; Nair et al., 2012; Moorthy et al., 2013; Pan et al., 2014) and East Asia (Park et al., 2005; Koch et al., 2009; Fu et al., 2012). The contribution of residential emissions is illustrated by the model simulation where these emissions are switched off, with substantially greater underestimation of BC (NMBF = −5.12), OC (NMBF = −11.46) and $PM_{2.5}$ (NMBF = −1.60) concentrations (Fig. 3d). Doubling residential carbonaceous emissions improves model agreement with observations, but the model still underestimates BC (NMBF = −1.33), OC (NMBF = −2.96) and $PM_{2.5}$ (NMBF = −1.17) concentrations.

Figure 4 compares observed and simulated concentrations for South Asian locations. The baseline simulation underestimates carbonaceous aerosol concentrations at all locations, although there is better agreement at Godavari and Hanimaadhoo. BC measurements at these two sites were made through thermal-optical methods, whereas other locations in South Asia used optical methods (Table 2). Different measurement

ACPD
15, 20449–20520, 2015

techniques result in different mass concentrations (Stone et al., 2007) and may contribute to model-observation errors. The emission inventory that we use is based on carbonaceous measurements using thermal-optical methods (Bond et al., 2004), which might explain the better agreement at Godavari and Hanimaadhoo. Doubling residential carbonaceous emissions improves the comparison against observations but leads to slight overestimation at Godavari and Hanimaadhoo. Pan et al. (2014) found that seven different global aerosol models underpredicted observed BC by up to a factor 10, suggesting that anthropogenic emissions are underestimated in these regions.

Observed BC and OC concentrations show strong seasonal variability, with lower concentrations during the summer monsoon period (June–September). The baseline simulation generally captures this seasonality relatively well (correlation coefficient between observed and simulated monthly mean concentrations $r > 0.5$ at most sites), with minimal improvement with monthly varying anthropogenic emissions. This suggests that metrological conditions such as enhanced wet deposition during the summer monsoon period are the dominant drivers for the observed and simulated seasonal variability, consistent with other modelling studies for the same region (Adhikary et al., 2007; Moorthy et al., 2013). Model simulations where RSF emissions have been switched off, shows that residential combustion contributes about two thirds of simulated BC and OC at these locations. Figure 4k–l shows a comparison of observed and simulated aerosol number concentrations at Hanimaadhoo. At this location, the baseline simulation well simulates N_{20} (NMBF = 0.14), N_{50} (NMBF = 0.14) and N_{100} (NMBF = 0.24) concentrations. Simulated number concentrations are sensitive to emitted particle size. Emitting residential primary carbonaceous emissions at very small sizes (res_small) results in an overestimation of N_{20} (NMBF = 1.84), N_{50} (NMBF = 1.28) and N_{100} (NMBF = 1.05), suggesting that this assumption is unrealistic.

Figure 5 compares observed and simulated surface monthly mean BC and OC concentrations for East Asian locations. Observed surface BC and OC concentrations are generally enhanced during winter (December–February) compared to the summer (June–August). At all locations, the model underestimates BC (except for Gosan)

ACPD
15, 20449–20520, 2015

and OC concentrations. The baseline simulation underpredicts both BC (NMBF < −2) and OC (NMBF < −6) at Gaolanshan and Longfengshan (and Akdala, Dunhuang and Wusumu, which are not shown in Fig. 5), which is consistent with a previous model study at these locations (Fu et al., 2012). The substantial underestimation at some locations (e.g., Dunhuang, Gaolanshan and Wusumu) may be due to local particulate sources that are not resolved by coarse model resolution. If we exclude these locations, NMBF improves for BC (−2.61 to −1.34) and OC (−4.43 to −3.29) for the East Asian region. The model better simulates BC (NMBF < −1) and OC (NMBF < −2) at Taiyangshan and Jinsha, although the model is still biased low. The baseline simulation, without seasonally varying emissions fails to capture the observed seasonal variability in East Asia, with negative correlations between observed and simulated aerosol concentrations at a number of locations. Fu et al. (2012) suggests that residential emissions (most likely heating sources) were the principle driver of simulated seasonal variability of EC (BC) at these locations. Implementing monthly varying anthropogenic emissions (including residential emissions) generally improves the simulated seasonal variability ($r > 0.3$ at most sites) compared to using annual mean emissions. Doubling residential carbonaceous emissions also leads to improved NMBF at most locations. Residential emissions typically account for 50–65 % of simulated BC and OC concentrations at these locations.

Figure 6 compares simulated and observed aerosol at Southern African and Eastern European locations. Marikana, Botsalano and Welgegund are all located within the same region of South Africa and are influenced by both residential emissions and open biomass burning during the dry season, of which open biomass burning savannah fire seasonality peaks in July–September (Venter et al., 2012; Vakkari et al., 2013). Simulated aerosol number concentrations (N_{20} and N_{100}) are underestimated at Marikana, consistent with the underprediction in BC at the same location, while number concentrations are better simulated at Botsalano and Welgegund. The model underprediction at Marikana is likely due to the location being closer to emission sources, compared to Botsalano and Welgegund. For N_{100} the model is generally good at simulating

ACPD
15, 20449–20520, 2015

open biomass savannah burning seasonality (peaking in August–September), but increases in observed N_{100} earlier in the season (May–August at Marikana and July at Welgegund) are not simulated. This earlier peak N_{100} is due to residential heating emissions at Marikana, and most likely also at Welgegund due to heating emission plume being transported 100 km from the Johannesburg-Pretoria megacity to the location, as well as from smaller nearby settlements (Vakkari et al., 2013), which suggests that residential emissions are underrepresented in the model possibly due to resolution effects. Aerosol number concentrations at Botsalano (NMBF = 0.47 to 1.01) and Welgegund (NMBF = 0.55 to 2.81) are overestimated when primary carbonaceous particles are emitted at the smallest size (res_small), matching comparisons in South Asia and further suggesting this assumption is unrealistic. The baseline simulation underestimates BC at Marikana (NMFB = −2.38) and $PM_{2.5}$ concentrations at Botsalano (NMBF = −0.88), with a reduction in BC bias when residential carbonaceous emissions are doubled (NMBF = −1.62). At both these locations the model simulates a reasonable seasonality even without monthly varying residential emissions ($r > 0.7$), possibly due to strong seasonality in open biomass savannah burning emissions.

Similar to other locations, observed BC and OC concentrations in Eastern Europe (Fig. 6i–l) are enhanced during winter (December–February). The baseline simulation performs well at simulating BC at Kosetice (NMBF= +0.07) and Iskrba (NMBF = −0.14) but underestimates OC at Kosetice (NMBF = −2.21) and Iskrba (NMBF = −3.27). Model agreement does not improve much when monthly varying anthropogenic emissions are used. The model performs better when residential carbonaceous emissions are doubled, but overestimates BC at Kosetice.

In summary, we find the model typically underestimates observed BC and OC mass concentrations matching results from previous studies. Doubling residential emissions improves comparison against BC and OC observations, although the model is still typically biased low. To explore this further, we use ^{14}C analysis (Sect. 3.2) to evaluate the contribution of residential emissions to carbonaceous aerosol. In general, the model

ACPD
15, 20449–20520, 2015

compares better against observations of particle number, except when carbonaceous particles are emitted at small sizes leading to large overestimates in particle number.

3.2 Contribution of residential emissions to PM concentrations

Figure 7 shows the fractional contribution of residential emissions to annual mean surface $PM_{2.5}$, BC, POM and sulfate concentrations for the baseline simulation. Greatest fractional contributions (15 to > 40 %) to surface $PM_{2.5}$ are simulated over Eastern Europe (including parts of the Russian Federation), parts of East Africa, South Asia and East Asia. Over these regions residential emissions contribute annual mean $PM_{2.5}$ concentrations of up to 6 $\mu g\,m^{-3}$ dominated by changes in POM concentrations of 2–5 $\mu g\,m^{-3}$, with BC and sulfate contributing up to 1 $\mu g\,m^{-3}$. Residential emissions contribute up to 60 % of simulated BC and POM over parts of Eastern Europe, Russian Federation, Asia, South East Africa and Northwest Africa. Contribution of residential emissions to surface sulfate concentrations are typically smaller, with contributions of 10–14 % over parts of Asia, Eastern Europe, Russian Federation where residential coal emissions are more important (see Sect. 2.2). Over China, residential emissions account for 13 % of simulated annual mean $PM_{2.5}$, with larger contributions of 20–30 % in the eastern China. Over India, residential emissions account for 22 % of simulated annual mean $PM_{2.5}$, with contributions > 40 % over the Indo-Gangetic Plain. The contributions to $PM_{2.5}$ are increased to 21 % for China and 34 % for India, when residential carbonaceous emissions are doubled. The contribution of residential emissions to annual mean surface BC (POM) concentrations is ~ 40 % (44 %) for China and ~ 60 % (58 %) for India. When residential carbonaceous emissions are doubled, BC (POM) contributions are increased to 55 % (60 %) for China and 75 % (73 %) for India.

The absolute contribution of residential emissions to PM concentrations are greatest in the NH between 0 and 60° N below 500 hPa (not shown). The fractional contributions within this region are up to 16–24 % for both BC and POM and 1–4 % for sulfate. Residential emissions contribute ~ 20 % of BC and ~ 12–16 % of POM aloft (above

ACPD
15, 20449–20520, 2015

500 hPa), but cause small reductions in sulfate (−1 to −4 %) due to the suppression of nucleation and growth (see Sect. 3.4 for more details).

Table 3 reports the impact of residential emissions on simulated global annual mean BC and POM burden, and continental surface $PM_{2.5}$ concentrations. In the baseline simulation, the global BC burden is 0.11 Tg with a global mean atmospheric BC lifetime of 4.95 days. This lifetime matches the 4.4 to 5.1 days reported by Wang et al. (2015b), suggesting that our underestimation of observed BC is not due to fast deposition and short atmospheric lifetime, at least in comparison to other models. In the baseline simulation, residential emissions result in a global BC burden of 0.024 Tg, contributing 22 % of the global BC burden. Residential emissions contribute 12 % of global POM burden. When residential carbonaceous emissions are doubled, residential emissions contribute 33 % of the BC burden and 23 % of the POM burden. Changing from annual mean to monthly varying emissions results in little change to the global BC or POM burden. Interestingly, emitting carbonaceous particles at very small sizes (res_small) results in a greater fractional contribution to global atmospheric BC (∼ 23 %) and POM (∼ 18 %) and longer BC lifetime (5.4 days) compared to the baseline simulation. Because the removal of carbonaceous particles in the model is size dependant (particularly for wet deposition), small particles below a critical size can escape removal leading to enhanced lofting to the free troposphere (FT), where deposition rates are slow. In the res_small simulation, fractional changes in BC burden can be as large as 60–100 % in the FT, compared to 25–40 % in the baseline simulation. Continental surface $PM_{2.5}$ concentrations are increased by ∼ 2 % in the baseline simulation, which is increased to ∼ 3.6 % when carbonaceous residential emissions are doubled. Distinct changes in $PM_{2.5}$ are seen only in simulations where residential emission mass have been changed, although small disenable changes are seen in experiments where carbonaceous particle have been emitted at different sizes due to either reduced removal (res_aero and res_small) or slightly enhanced removal (res_large) rates.

We further evaluate the simulated contribution of residential emissions to BC concentrations using ^{14}C source apportionment studies on the island of Hanimaadhoo

ACPD
15, 20449–20520, 2015

(Gustafsson et al., 2009; Sheesley et al., 2012; Bosch et al., 2014), which is influenced by pollution transported from the Indian subcontinent. The model well simulates both BC and OC concentrations observed at this location (Sect. 3.1). Figure 8 compares simulated and observed biomass contributions to BC at Hanimaadhoo. The observed contribution depends on the time of year and the measurement technique used to derive BC (EC). Gustafsson et al. (2009) concluded 46 ± 8 % of EC and 68 ± 6 % of BC originated from non-fossil biomass (January–March). Bosch et al. (2014) estimate that 59 ± 8 % of EC is from non-fossil biomass (February–March). Sheesley et al. (2012) estimated that 73 ± 6 % of BC originated from non-fossil biomass during the dry season (November–February). The observed contribution is therefore lower for EC measurements (46–59 %) compared to BC measurements (68–73 %), with slightly greater contribution in the November–February (73 %) compared to January to March (68 %). Residential biofuel/biomass (e.g., including wood, charcoal, animal waste and agricultural residues) combustion dominates residential emissions in South Asia (Venkataraman et al., 2005). To estimate non-fossil values from the model, we assume that 90 % of residential BC transported to Hanimaadhoo originates from residential biofuel sources (consistent with ≥ 90 % estimate from the GAINS model), while the remaining non-fossil BC originates from open biomass burning. We find a small contribution (< 10 % for all simulations) of open biomass burning to simulated BC at Hanimaadhoo, confirming that the non-fossil contribution at this location is likely dominated by residential biomass/biofuel sources, which is supported by the observed consistent contribution from a non-fossil source (Sheesley et al., 2012). The simulated contribution of non-fossil sources to total BC at this location is ∼ 57–79 %, depending on the time of year and model simulation. The baseline simulation has a 57 % contribution of non-fossil sources to simulated BC concentrations, with little variation between different times of year due to the annual mean emissions applied in this simulation. Model simulations with monthly varying emissions have a greater contribution of non-fossil sources to BC at this location, as well as greater variability between seasons with a contribution of 62–65 %. Doubling residential emissions increases the contribution of non-fossil sources to

ACPD
15, 20449–20520, 2015

~ 72 % for annual mean emissions and ~ 76–79 % for monthly varying emissions. The different measurement methods make it difficult to constrain the contribution of residential emissions: the baseline emissions are more consistent with EC observations whereas doubling residential emissions are more consistent with BC observations. We do not analyse the non-fossil fraction of OC since OC arises from a larger range of sources including primary emissions and secondary organic aerosol (SOA). Nevertheless, non-fossil water soluble organic carbon at Hanimaadhoo is dominated (~ 80 %) by biomass and biogenic sources (Kirillova et al., 2013) during the same time periods, with the relative enrichment in the stable ($^{\delta}$13C) carbon isotope points largely to aged primary biomass emissions (Bosch et al., 2014). We estimate the simulated biomass contribution to OC at Hanimaadhoo to be ~ 50–70 % for baseline simulations (res_base and res_monthly) and ~ 70–80 % for simulations where residential carbonaceous emissions have been doubled.

3.3 Health impacts of residential emissions

Figure 9 shows the simulated annual excess premature mortality due to exposure to ambient $PM_{2.5}$ from residential emissions in the year 2000 for the baseline simulation. Greatest mortality is simulated over regions with substantial residential emissions and high population densities, notably parts of Eastern Europe, the Russian Federation, South Asia and East Asia. Table 3 reports total global values for annual mortality due to residential emissions. For the baseline simulation, we estimate a total global annual mortality of 315 000 (132 000–508 000, 5th to 95th percentile uncertainty range). The simulation with monthly varying emissions (res_monthly) results in total global annual mortality of 308 000 (113 300–497 000), only a 8 % difference from the baseline estimate. Uncertainty in the magnitude of residential emissions causes substantial uncertainty in the simulated impact on human health. When residential carbonaceous emissions are doubled, annual premature mortality increases by 65 % to 519 000 (193 000–830 000) with annual mean emissions, and by 68 % to 517 000 (192 000–827 000) with monthly varying emissions. Therefore, uncertainty in the emission bud-

ACPD
15, 20449–20520, 2015

get and uncertainty in the health impacts of PM (as specified by 95 % confidence intervals in the cause-specific coefficients) result in similar uncertainties in estimated global mortality. Factorial simulations where residential emissions of POM, BC and SO_2 are increased individually shows that health effects are most sensitive to uncertainty in POM emissions which dominates the total emission mass. Doubling POM emissions (res_POM×2) increases estimated premature mortality by 50 %, whereas doubling BC emissions (res_BC×2) results in an 11 % increase and doubling SO_2 emissions (res_SO2×2) leads to a 6.5 % increase.

Figure 10 shows simulated annual total mortality by region. For the baseline simulation, we estimate that residential emissions cause the greatest mortality in East Asia with 121 075 (44 596–195 443, 95 % confidence intervals) annual deaths – 38 % of global mortalities due to residential emissions. We also calculate substantial health effects in other regions, with 72 890 (26 891–117 360) annual deaths in South Asia (28 % of global mortalities) and 69 757 (25 714–112 447) in Eastern Europe and Russia (22 % of global mortalities). Elsewhere we estimate lower mortality with 16 723 (6152–27 018) annual deaths in Southeast Asia (5 %) and 4791 (1751–7784) in sub-Saharan Africa (2 %). Annual premature mortality in sub-Saharan Africa is less than in Asia due to a smaller contribution of residential emissions to $PM_{2.5}$ concentrations (Fig. 7), combined with typically lower population densities, lower baseline mortality rates for lung cancer and cardiopulmonary disease and smaller fraction of the population over 30 years of age.

To our knowledge, this is the first study of the global excess mortality due to ambient $PM_{2.5}$ from residential cooking and heating emissions. A recent study by Chafe et al. (2014) concluded that ambient $PM_{2.5}$ from RSF cooking emissions resulted in 420 000 annual excess deaths in 2005 and 370 000 annual excess deaths in 2010. Chafe et al. (2014) also simulated lower mortality in sub-Saharan Africa (10 800 deaths in 2005) compared to Asia, consistent with our findings. The regions where we estimate the largest health impacts due to residential emissions are dominated by RSF emissions. In East Asia, residential emissions are dominated by both residential coal and

ACPD
15, 20449–20520, 2015

biofuel sources whereas in South Asia emissions are dominated by biofuel sources (Bond et al., 2013).

3.4 Impact of residential emissions on total particle number and CCN concentrations

Figure 11 shows the change in annual mean surface and zonal mean particle number concentration (N_3; particles greater than 3 nm dry diameter) due to residential emissions for the baseline simulation. Residential emissions increase N_3 concentrations over source regions by up to 800 cm^{-3} due to primary emitted particles. Downwind of source regions, N_3 concentrations are reduced by up to $\sim$ 400 cm^{-3}. This reduction is caused by primary particles acting as a coagulation sink for nucleated particles and a condensation sink for nucleating and condensing vapors, suppressing new particle formation (Spracklen et al., 2006). Residential emissions decrease N_3 concentrations in the FT (> 500 hPa) by up to 100 cm^{-3} (7 %) due to suppression of nucleation and growth from reduced availability of H_2SO_4 vapour due to increased condensation on primary particles.

In the baseline simulation, residential emissions reduce annual global mean N_3 concentrations by 1.0 % (Table 3). When activation BLN is switched off (res_BHN), this suppression is no longer important, and residential emissions increase annual global mean N_3 concentrations by 5.7 %. The impact of residential emissions on global particle number depends on the assumed particle size of primary carbonaceous emissions. When residential carbonaceous emissions are emitted at smaller sizes (res_aero and res_small), global mean N_3 concentrations are increased by 2.4 and 164 %, respectively. This is because a greater number of particles are being emitted per emission mass compared to the baseline simulation.

Figure 12 shows the impact of residential emissions on surface and zonal mean CCN number concentrations (soluble N_{50}) for the baseline simulation. Residential emissions increase CCN concentrations over source regions of East Asia, South Asia and Eastern

ACPD
15, 20449–20520, 2015

Europe by up to 300–500 cm^{-3}. Simulated CCN concentrations are increased by up to 20 % in the Arctic, Eastern Europe, Russian Federation, North Africa and South Asia. Despite high absolute changes, fractional changes in CCN concentration over East Asia (e.g., China) are smaller (< 15 %) because of higher baseline CCN in this region from other sector emissions (e.g., from industry). CCN concentrations increase globally due to residential emissions, but small reductions (< 5 %) are simulated in the remote Southern Ocean because of the reduction in the amount of H_2SO_4 and condensable vapour available for nucleation and growth in FT, which results in reduced entrainment of nucleated particles into the boundary layer. Absolute and fractional changes in zonal mean CCN are greatest between 0 and 60° N and below 500 hPa.

Table 3 reports the global annual mean change in CCN concentrations between different simulations. In the baseline simulation, residential emissions increase global mean surface CCN by ∼ 5 %. When primary residential carbonaceous particles are emitted at smaller sizes, residential emissions cause a greater increase in CCN concentrations, with annual global mean CCN concentrations increasing by ∼ 20 % in the simulation with smallest particle size (res_small). Emitting particles at larger sizes results in smaller increase in global mean CCN (3.1 %) because large particles are more efficiently scavenged. The sensitivity of global mean CCN concentrations to assumptions about emitted particle size is consistent with previous studies (Adams and Seinfeld, 2003; Spracklen et al., 2005b, 2011a). When residential carbonaceous aerosol emissions are doubled, residential emissions increase global annual mean CCN by ∼ 6.3 % (res_×2). Simulations where individual carbonaceous components are doubled separately (res_BC×2 and (res_POM×2) show that CCN is mainly sensitive to change in OC emissions which dominate the carbonaceous aerosol mass. When residential SO_2 emissions are doubled, residential emissions increase global annual mean CCN by 6.5 %. When activation BLN is assumed not to occur, residential emissions increase global annual mean CCN by 6.5 % relative to the simulation with no residential emissions. This greater sensitivity is because the baseline CCN concentrations without BLN are lower (287.4 cm^{-3}), compared to the baseline simulation (364.6 cm^{-3}).

ACPD
15, 20449–20520, 2015

3.5 Impact of residential emissions on cloud droplet number concentrations

Figure 13 shows the impact of residential emissions on annual mean low-cloud level (850–900 hPa) and zonal mean CDNC for the baseline simulation. Residential emissions increase low-cloud level CDNCs by 20–100 cm^{-3} over source regions. Smaller absolute and percentage changes in CDNC are simulated over regions with greater baseline CDNCs, due to CDNC saturation effects. In contrast, CDNCs increases of 20 % are simulated over regions with low simulated background CDNCs, including parts of East Africa. Simulated absolute increases in zonal mean CDNC are greatest between 0 and 60° N below 500 hPa, whereas greatest fractional changes occur in the Arctic (6–8 %) due to low background concentrations. Small reductions in CDNC are simulated in the FT (∼ −2 %) and in the remote Southern Oceans (1–2 %) at cloud level. This is caused by suppressed nucleation in the FT.

In the baseline simulation, residential emissions increase global annual low-cloud level CDNC by 2.1 % (Table 3). Uncertainty in the emitted particle size of primary carbonaceous emissions causes most of the uncertainty in simulated CDNC. When residential carbonaceous particles are emitted at smaller sizes (res_small) emissions increase global annual mean CDNC by 20 %. Emitting particles at smaller sizes resulted in greater N50 concentrations, meaning more CCN-sized particles are available to activate. While larger particle sizes can active cloud drops more easily compared to smaller particles, large particles will deplete available water vapour more quickly, which will lower SS_{max} leading to a suppression of small particles being activated. When activation BLN is switched off (res_BHN), residential emissions cause a greater increase in CDNC (3 %) compared to the baseline simulation, due to lower background CDNCs. Annual mean CDNC are increased by +2.7 % when primary carbonaceous emissions are doubled (res_×2), but greater increases (+3.3 %) are simulated when residential SO_2 is doubled separately (res_SO2×2). This suggests that residential SO_2 is having a greater effect on CDNC compared to carbonaceous emissions because the small size distribution of secondary sulfate is more efficient in the activation of cloud drops.

ACPD
15, 20449–20520, 2015

3.6 Radiative effects of residential emissions

Figure 14 shows annual mean all-sky TOA DRE and first AIE due to residential emissions for the baseline simulation. Residential emissions result in a negative (cooling) annual mean DRE over large regions of South Asia, East Asia, Sub Saharan Africa and parts of Southern Europe, with values as large as $-200\,\mathrm{mW\,m^{-2}}$. The simulated net negative DRE in South Asia and East Asia is consistent with a previous study (Aunan et al., 2009). In contrast, over parts of Eastern Europe and the Russian Federation, North Africa, the Middle East, and South East Asia, residential emissions lead to a positive DRE. Residential emissions cause a negative first AIE over most regions, with values as large as $-200\,\mathrm{mW\,m^{-2}}$ over East Africa, Eastern Europe and West Africa. Small positive AIE ($< 40\,\mathrm{mW\,m^{-2}}$) are simulated in the remote Southern Ocean, due to reductions in CDNC as mentioned in Sect. 3.5.

Figure 15 compares the annual mean all-sky DRE and first AIE across the different model simulations (also reported in Table 3). The simulated global annual mean DRE has an uncertain sign, with our estimates between -66 and $+85\,\mathrm{mW\,m^{-2}}$. The baseline simulation results in a global mean DRE of $-5\,\mathrm{mW\,m^{-2}}$, similar to the simulation using monthly varying emissions ($-8\,\mathrm{mW\,m^{-2}}$). Doubling residential carbonaceous emissions, but keeping SO_2 emissions constant, results in a positive global annual mean DRE ($+21\,\mathrm{mW\,m^{-2}}$ for res_×2 and $+10\,\mathrm{mW\,m^{-2}}$ for res_monthly_×2). This suggests that the carbonaceous (BC and POM) component of residential aerosol in our model exerts a positive DRE, but that this is offset by cooling from SO_2 emissions. Doubling only BC emissions leads to a stronger positive DRE ($+85\,\mathrm{mW\,m^{-2}}$), whereas negative DRE are simulated for doubling only POM ($-66\,\mathrm{mW\,m^{-2}}$) or SO_2 ($-43\,\mathrm{mW\,m^{-2}}$) emissions. The DRE is also sensitive to emitted particle size, resulting in positive global mean DRE of between +1 and $+63\,\mathrm{mW\,m^{-2}}$ when carbonaceous particles are emitted at smaller sizes (res_aero and res_small, respectively). This change in sign to a positive DRE can be attributed to reduced removal rates for carbonaceous particles emitted at smaller sizes, which leads to larger BC burden, particularly in the FT where BC in-

ACPD
15, 20449–20520, 2015

fluence on DRE is most efficient. Residential emissions exert a negative (cooling) but uncertain global annual mean first AIE, estimated at between −502 and −16 mW m^{-2}. The baseline simulation results in a global mean first AIE of −25 mW m^{-2}, similar to the simulation using monthly varying emissions (−20 mW m^{-2}). Emitting residential carbonaceous aerosol at small sizes contributes most of the uncertainly to simulated first AIE, with estimates between −46 mW m^{-2} (res_aero) and −502 mW m^{-2} (res_small) due to a greater increase in global CDNC. We find little sensitivity of the AIE to changes in carbonaceous emission mass: doubling carbonaceous emissions (res_×2) changes AIE by less than 2 mW m^{-2} (∼ 10 %), due to limited changes in CDNC. In contrast doubling SO_2 emissions, leads to the greater negative AIE (−45 mW m^{-2}) due to greater global contribution to CDNCs.

4 Discussion and conclusions

We used a global aerosol microphysics model (GLOMAP) to quantify the impacts of residential emissions on ambient aerosol, human health and climate in the year 2000. We tested the sensitivity of simulated aerosol to uncertainty in emission amount and seasonal variability, emitted primary carbonaceous aerosol size distributions and the impact of particle formation.

To evaluate model simulations we synthesised in-situ observations of BC, OC and $PM_{2.5}$ concentrations, and aerosol number size distribution. The baseline simulation underestimated observed BC, OC and $PM_{2.5}$ concentrations, with largest underestimation over East Asia and South Asia, consistent with other modelling studies (Fu et al., 2012; Moorthy et al., 2013; Pan et al., 2014). Applying monthly varying emissions (MACCity emission dataset), in place of annual mean emissions (ACCMIP emission), has little improvement on overall model bias, but improves the ability of the model to simulate the observed seasonal variability of aerosol. Doubling residential carbonaceous combustion emissions, improved model agreement, but GLOMAP still underestimated BC, OC and $PM_{2.5}$ concentrations. The model typically had a larger

ACPD
15, 20449–20520, 2015

underestimation of OC compared to BC concentrations, possibly due to uncertainty in emission factors for residential emissions or potentially due to an underestimation of SOA (Spracklen et al., 2011b).

We used source apportionment studies using ^{14}C non-fossil BC analysis at the island site of Hanimaadhoo in the Indian Ocean as an additional constraint of the model. Different observational methods (e.g., thermo-optical EC and optical BC) result in substantial uncertainty in the contribution of non-fossil BC sources to total BC concentrations, with estimates ranging from 46–59 % for EC methods and 68–73 % for BC methods. This makes it difficult to use these observations to constrain the contribution from residential biomass sources. With standard emissions (ACCMIP and MACCity), we simulate a non-fossil fraction of 57–65 %, more consistent with EC observations. When residential emissions are doubled we simulate a non-fossil fraction of 72–79 %, more consistent with BC observations. Overall, our results suggest that residential emissions may be underestimated in the MACCity and ACCMIP datasets. Previous modelling studies have also suggested that residential emission datasets underestimate emissions (Park et al., 2005; Koch et al., 2009; Ganguly et al., 2009; Menon et al., 2010; Bergström et al., 2012; Nair et al., 2012; Fu et al., 2012; Moorthy et al., 2013; Bond et al., 2013; Pan et al., 2014). The ACCMIP and MACCity emission datasets are constructed using national data on fuel use, which implies uniform per capita fuel consumption at the country level. Using subnational fuel use data, R. Wang et al. (2014) showed that the MACCity dataset underestimated residential emissions over source regions in Asia. Other studies have also had to increase residential emissions over Europe in order to match source apportionment studies (Denier van der Gon et al., 2015). On the other hand, Wang et al. (2013) suggested that model bias over China could partly be attributed to coarse model resolution and comparison against urban data and monthly mean observations. Kumar et al. (2015) also showed that a high resolution model was able simulate reasonable BC distributions in South Asian region. We have restricted our analysis to rural and background sites, but use monthly mean BC and OC data and a relatively coarse resolution global model. To help resolve uncertainties in

ACPD
15, 20449–20520, 2015

residential emission budget, higher resolution emission inventories (using subnational fuel use data) and higher resolution model simulations are required in combination with evaluation against a variety of long-term and high-time observational measurements. In many regions observational data is lacking; there is an urgent requirement for detailed characterisation of the chemical, physical and optical properties of aerosol in regions impacted by residential emissions particularly in the developing world.

Particle number concentrations are generally predicted within a factor 2 at the limited number of locations where observations are available. Simulated particle number is very sensitive to emitted particle size, which has a large uncertainty. Emitting residential carbonaceous particles at the small end of the range reported by Bond et al. (2006) (geometric mean diameter = 20 nm) substantially overestimates observed particle number, suggesting this assumption is not appropriate for coarse resolution global models.

Residential emissions contribute substantially to simulated annual mean surface PM concentrations. Greatest fractional contributions (15 to > 40 %) to surface $PM_{2.5}$ concentrations are simulated over Eastern Europe (including parts of the Russian Federation), parts of East Africa, South Asia and East Asia. In these regions residential emissions contribute > 50 % to total simulated BC and POM concentrations. These findings support previous studies suggesting a large contribution of residential emissions to $PM_{2.5}$ concentrations over Asia (Venkataraman et al., 2005; Cao et al., 2006; Klimont et al., 2009; Lei et al., 2011; Cui et al., 2015; Fu et al., 2012; Gustafsson et al., 2009; Chen et al., 2013a). Our findings suggest that reductions in residential emissions need to be considered alongside mitigation strategies for other PM sources (e.g., industry and transport) within Asia, and even more developed regions such as in parts of Europe (Fountoukis et al., 2014).

We estimated the impact of residential emissions on human health due to increased ambient $PM_{2.5}$ concentrations and tested sensitivity to the emission dataset and emission budget. We used a log-linear model of relative risk from the epidemiological literature (Ostro, 2004) to relate simulated changes in ambient $PM_{2.5}$ concentrations to

ACPD
15, 20449–20520, 2015

long-term excess premature mortality for cardiopulmonary disease and lung cancer for adults (> 30 years of age). In the baseline simulation, we estimate that residential emissions cause 315 000 (132 000–508 000, 5th to 95th percentile uncertainty range) premature mortalities each year. Applying a seasonal cycle to emissions changed our estimate by less than 2 %, with residential emissions resulting in 308 000 (113 300–497 000) premature mortalities each year. Our estimate for residential emissions is equivalent to 8 % of the total mortality attributed to exposure to ambient $PM_{2.5}$ from all anthropogenic sources (WHO, 2014b), although we note that methodologies in the two studies are different. Doubling residential carbonaceous emissions, which improved model comparison against observed BC and POM concentrations, increases simulated excess mortality by ~ 64 % to 516 600 (192 000–827 000). Simulated mortality is greatest over regions with large residential emissions and high population densities including East Asia and South Asia, Eastern Europe and the Russian Federation. We find that half of simulated global excess mortality from residential emissions occurs in China and India alone. Our results are consistent with a previous estimate of RSF cooking emissions on premature mortality (Chafe et al., 2014). The CRFs that are used to estimate long-term premature mortality are uncertain. The log-linear function used here is based on epidemiological studies from North America (Pope III et al., 2002), resulting in greater uncertainty when these functions are extrapolated to other regions (Silva et al., 2013). However, epidemiological studies are not available for all regions, so global mortality estimates often use functions based on these North American studies. Overall, we find that uncertainty in the relationship between PM concentrations and health impacts (as quantified by the 95th percentile range given by the log-linear model) and our measure of uncertainty in emissions (estimated here as a factor of 2 uncertainty) result in comparable uncertainty in the estimated global number of premature mortalities. Future work therefore needs to improve both our understanding of residential emissions and the relationships between enhanced PM concentrations and human health impacts. Higher resolution simulations will be required to accurately simulate $PM_{2.5}$ concentrations in urban and semi-urban areas and associated health

ACPD
15, 20449–20520, 2015

effects using more recent CRFs that relate RR of disease to changes in $PM_{2.5}$ over a large range of concentration exposures (Burnett et al., 2014).

We used an offline radiative transfer model to estimate the radiative effect (RE) of aerosol from residential emissions. We estimate that residential emissions exert a global annual mean direct radiative effect (DRE) of between −66 and +85 $mW\,m^{-2}$. The simulated global mean DRE is sensitive to the ratio of BC, POM and SO_2 in emissions. Doubling residential carbonaceous emissions, but keeping SO_2 emissions constant, results in a positive global annual mean DRE, suggesting that the carbonaceous component of residential aerosol exerts a net positive DRE in our simulations, offset by cooling from SO_2 emissions. We also find a positive DRE when primary carbonaceous emissions are emitted at smaller sizes, but this simulation overestimates observed aerosol number, suggesting it is unrealistic. Discounting this simulation, we provide a best estimate of global mean DRE due to residential combustion of between −66 and +21 $mW\,m^{-2}$ for the year 2000.

Residential emissions exert a simulated global annual mean first aerosol indirect effect (AIE) of between −502 and −16 $mW\,m^{-2}$. Uncertainty in emitted primary carbonaceous particle size contributes most of the uncertainly to calculated AIE. Emitting carbonaceous aerosol at smaller sizes results in greater simulated CCN and CDNC and a strong negative AIE, but results in overestimation of observed particle number, suggesting that emission at very small sizes is not realistic. We find little sensitivity to annual mean first AIE due changes in carbonaceous emission mass compared to the baseline simulation. Doubling carbonaceous emissions, changes AIE by less than 2 $mW\,m^{-2}$ (∼ 10 %), highlighting a non-linear relationship between magnitude of emission and first AIE. Our best estimate of the first AIE due to residential emissions is between −52 and −16 $mW\,m^{-2}$ in the year 2000.

We have restricted our analysis of the RE of residential emissions to the aerosol DRE and first AIE. We treat POM aerosol as scattering, although a fraction of POM aerosol may absorb radiation (Kirchstetter et al., 2004; Chen and Bond, 2010; Arola et al., 2011; X. Wang et al., 2014). Furthermore, BC particles coated in a non-absorbing

ACPD
15, 20449–20520, 2015

shell produce stronger absorption than the BC core alone (Jacobson, 2001), which we do not treat here. Because we use an offline radiative transfer model, we also do not treat cloud lifetime (second indirect effect) or semi-direct effects (Koch and Del Genio, 2010), and cannot explore additional impacts such as the weakening of the South Asia monsoon, altering of precipitation patterns (Ramanathan et al., 2005), tropical cyclone intensification (Evan et al., 2011), and accelerated melting of glaciers in the Himalayas (Xu et al., 2009).

The introduction of cleaner and fuel efficient residential combustion technologies, processed solid fuels, and clean alternative energy (e.g., natural gas, electricity etc.) has been suggested as one of the fastest ways to reduce RSF emissions (UNEP, 2011), thus slowing climate change and improving air quality and human health (WHO, 2009). Our study shows that the complete elimination of residential emissions would result in substantially improved PM air quality and human health across large regions of the world regardless of the uncertainties between the different model simulations explored here.

We have shown that residential combustion emissions exert an uncertain RE, which leads to uncertainties in predicting the climate impact of emission reductions. Our work suggests that residential emission flux, chemical composition and carbonaceous size distributions need to be better characterised in order to constrain the likely climate impact. Given these uncertainties, the missing processes within our model framework (described above), and the use of an offline radiative transfer model, it is difficult asses the full climate impacts due to residential emissions. In addition, because we find residential emission amount and resulting RE (particularly aerosol-cloud effects) are not linearly related, our results cannot be used to estimate the impacts associated with smaller, realistic reductions in residential emissions. Future research is needed to explore the air quality and climate impact of realistic emission reductions scenarios that could potentially be achieved through the implementation of cleaner combustion technologies and clean alternative fuels.

ACPD
15, 20449–20520, 2015

More people are using RSF for cooking than at any other point in human history, even though the fraction of the population using these fuels is falling (Bonjour et al., 2013). Over the next few decades (2005–2030), combustion of RSF is projected to increase in South Asia and Africa due to increases in human population (UNEP, 2011). In China, emissions from the residential sector have increased 34 % during the period 2000–2012 due to the growth of coal consumption (Cui et al., 2015). The use of biomass for heating is also expected to increase in developed countries such as in Western Europe because of rising fossil fuel prices and use of renewable biomass under climate change mitigation policy (Denier van der Gon et al., 2015). The impact of residential emissions on human health and climate is therefore likely to persist in the future, unless effective mitigation to address the dependence on RSFs is taken.

Acknowledgements. E. W. Butt acknowledges support from the United Bank of Carbon and the University of Leeds. V. Vakkari acknowledges support from the Academy of Finland Finnish Center of Excellence program (grant 1118615). Ambient aerosol measurements obtained through the Atmospheric Brown Cloud project funded by the United Nations Environmental Programme and the National Oceanic and Atmospheric Administration. Particulate matter sample collection, analysis, and data validation was supported by James J. Schauer at the University of Wisconsin-Madison, Jeff DeMinter at the Wisconsin State Laboratory of Hygiene, Soon-Chang Yoon of Seoul National University, Pradeep Dangol and Bidya Banmali Pradhan at the International Center for Integrated Mountain Development. We acknowledge funding from the Natrual Environment Research Council (NERC).

References

Adams, P. and Seinfeld, J.: Disproportionate impact of particulate emissions on global cloud condensation nuclei concentrations, Geophys. Res. Lett., 30, 1239, doi:10.1029/2002GL016303, 2003.

Adhikary, B. ,Carmichael, G. R., Tang, Y., Leung, L. R., Qian, Y., Schauer, J. J., Stone, E. A., Ramanathan, V., and Ramana, M. V.: Characterization of the seasonal cycle of south

ACPD
15, 20449–20520, 2015

Asian aerosols: a regional-scale modeling analysis, J. Geophys. Res.-Atmos., 112, D22S22, doi:10.1029/2006JD008143,2007.
Allen, R. W., Gombojav, E., Barkhasragchaa, B., Byambaa, T., Lkhasuren, O., Amram, O., Takaro, T. K., and Janes, C. R.: An assessment of air pollution and its attributable mortality in Ulaanbaatar, Mongolia, Air Quality, Atmosphere and Health, 6, 137–150, 2013.
Andres, R. and Kasgnoc, A.: A time-averaged inventory of subaerial volcanic sulfur emissions, J. Geophys. Res.-Atmos., 103, 25251–25261, 1998.
Anenberg, S. C., Horowitz, L. W., Tong, D. Q., and West, J.: An estimate of the global burden of anthropogenic ozone and fine particulate matter on premature human mortality using atmospheric modeling, Environ. Health Persp., 118, 1189–1195, 2010.
Arnold, S. R., Chipperfield, M. P., and Blitz, M. A.: A threedimensional model study of the effect of new temperaturedependent quantum yields for acetone photolysis, J. Geophys. Res., 110, D22305, doi:10.1029/2005jd005998, 2005.
Arola, A., Schuster, G., Myhre, G., Kazadzis, S., Dey, S., and Tripathi, S. N.: Inferring absorbing organic carbon content from AERONET data, Atmos. Chem. Phys., 11, 215–225, doi:10.5194/acp-11-215-2011, 2011.
Aunan, K., Berntsen, T. K., Myhre, G., Rypdal, K., Streets, D. G., Woo, J.-H., and Smith, K. R.: Radiative forcing from household fuel burning in Asia, Atmos. Environ., 43, 5674–5681, 2009.
Barahona, D., West, R. E. L., Stier, P., Romakkaniemi, S., Kokkola, H., and Nenes, A.: Comprehensively accounting for the effect of giant CCN in cloud activation parameterizations, Atmos. Chem. Phys., 10, 2467–2473, doi:10.5194/acp-10-2467-2010, 2010.
Bauer, S. E., Menon, S., Koch, D., Bond, T. C., and Tsigaridis, K.: A global modeling study on carbonaceous aerosol microphysical characteristics and radiative effects, Atmos. Chem. Phys., 10, 7439–7456, doi:10.5194/acp-10-7439-2010, 2010.
Bellouin, N., Rae, J., Jones, A., Johnson, C., Haywood, J., and Boucher, O.: Aerosol forcing in the Climate Model Intercomparison Project (CMIP5) simulations by HadGEM2-ES and the role of ammonium nitrate, J. Geophys. Res.-Atmos., 116, D20206, doi:10.1029/2011JD016074, 2011.
Bellouin, N., Mann, G. W., Woodhouse, M. T., Johnson, C., Carslaw, K. S., and Dalvi, M.: Impact of the modal aerosol scheme GLOMAP-mode on aerosol forcing in the Hadley Centre Global Environmental Model, Atmos. Chem. Phys., 13, 3027–3044, doi:10.5194/acp-13-3027-2013, 2013.

ACPD
15, 20449–20520, 2015

Bergström, R., Denier van der Gon, H. A. C., Prévôt, A. S. H., Yttri, K. E., and Simpson, D.: Modelling of organic aerosols over Europe (2002–2007) using a volatility basis set (VBS) framework: application of different assumptions regarding the formation of secondary organic aerosol, Atmos. Chem. Phys., 12, 8499–8527, doi:10.5194/acp-12-8499-2012, 2012.

Bond, T. C., Streets, D. G., Yarber, K. F., Nelson, S. M., Woo, J.-H., and Klimont, Z.: A technology-based global inventory of black and organic carbon emissions from combustion, J. Geophys. Res., 109, D14203, doi:10.1029/2003jd003697, 2004.

Bond, T. C., Habib, G., and Bergstrom, R. W.: Limitations in the enhancement of visible light absorption due to mixing state, J. Geophys. Res., 111, D20211, doi:10.1029/2006JD007315, 2006.

Bond, T. C., Bhardwaj, E., Dong, R., Jogani, R., Jung, S., Roden, C., Streets, D. G., and Trautmann, N. M.: Historical emissions of black and organic carbon aerosol from energy-related combustion, 1850–2000, Global Biogeochem. Cy., 21, GB2018, doi:10.1029/2006GB002840, 2007.

Bond, T. C., Doherty, S. J., Fahey, D., Forster, P., Berntsen, T., DeAngelo, B., Flanner, M., Ghan, S., Kärcher, B., and Koch, D.: Bounding the role of black carbon in the climate system: a scientific assessment, J. Geophys. Res.-Atmos., 118, 5380–5552, 2013.

Bonjour, S., Adair-Rohani, H., Wolf, J., Bruce, N. G., Mehta, S., Pruss-Ustun, A., Lahiff, M., Rehfuess, E. A., Mishra, V., and Smith, K. R.: Solid fuel use for household cooking: country and regional estimates for 1980–2010, Environ. Health Persp., 121, 784–790, 2013.

Bosch, C., Andersson, A., Kirillova, E. N., Budhavant, K., Tiwari, S., Praveen, P., Russell, L. M., Beres, N. D., Ramanathan, V., and Gustafsson, Ö: Source-diagnostic dual-isotope composition and optical properties of water-soluble organic carbon and elemental carbon in the South Asian outflow intercepted over the Indian Ocean, J. Geophys. Res.-Atmos., 119, 11743–11759, 2014.

Boucher, O., Randall, D., Artaxo, P., Bretherton, C., Feingold, G., Forster, P., Kerminen, V.-M., Kondo, Y., Liao, H., and Lohmann, U.: Clouds and aerosols, in: Climate Change 2013: The Physical Science Basis, Contribution of working group I to the fifth assessment report of the intergovernmental panel on climate change, Cambridge University Press, Cambridge, UK, and New York, NY, USA, 571–657, 2013.

Brook, R. D., Rajagopalan, S., Pope, C. A., Brook, J. R., Bhatnagar, A., Diez-Roux, A. V., Holguin, F., Hong, Y., Luepker, R. V., and Mittleman, M. A.: Particulate matter air pollution

ACPD
15, 20449–20520, 2015

and cardiovascular disease an update to the scientific statement from the American Heart Association, Circulation, 121, 2331–2378, 2010.
Browse, J., Carslaw, K. S., Arnold, S. R., Pringle, K., and Boucher, O.: The scavenging processes controlling the seasonal cycle in Arctic sulphate and black carbon aerosol, Atmos. Chem. Phys., 12, 6775–6798, doi:10.5194/acp-12-6775-2012, 2012.
Burnett, R. T., Pope, C. A., Ezzati, M., Olives, C., Lim, S. S., Mehta, S., Shin, H. H., Singh, G., Hubbell, B., and Brauer, M.: An integrated risk function for estimating the global burden of disease attributable to ambient fine particulate matter exposure, Environ. Health Perspect., 122, 397–403, doi:10.1289/ehp.1307049, 2014.
Cao, G., Zhang, X., and Zheng, F.: Inventory of black carbon and organic carbon emissions from China, Atmos. Environ., 40, 6516–6527, 2006.
Chafe, Z. A., Brauer, M., Klimont, Z., Van Dingenen, R., Mehta, S., Rao, S., Riahi, K., Dentener, F., and Smith, K. R.: Household cooking with solid fuels contributes to ambient $PM_{2.5}$ air pollution and the Burden of Disease, Environ. Health Perspect., 122, 1314–1320, 2014.
Chen, B., Andersson, A., Lee, M., Kirillova, E. N., Xiao, Q., Kruså, M., Shi, M., Hu, K., Lu, Z., and Streets, D. G.: Source forensics of black carbon aerosols from China, Environ. Sci. Technol., 47, 9102–9108, 2013.
Chen, Y. and Bond, T. C.: Light absorption by organic carbon from wood combustion, Atmos. Chem. Phys., 10, 1773–1787, doi:10.5194/acp-10-1773-2010, 2010.
Chen, Y., Sheng, G., Bi, X., Feng, Y., Mai, B., and Fu, J.: Emission factors for carbonaceous particles and polycyclic aromatic hydrocarbons from residential coal combustion in China, Environ. Sci. Technol., 39, 1861–1867, 2005.
Chen, Y., Zhi, G., Feng, Y., Fu, J., Feng, J., Sheng, G., and Simoneit, B. R.: Measurements of emission factors for primary carbonaceous particles from residential raw-coal combustion in China, Geophys. Res. Lett., 33, L20815, doi:10.1029/2006GL026966, 2006.
Chen, Y., Ebenstein, A., Greenstone, M., and Li, H.: Evidence on the impact of sustained exposure to air pollution on life expectancy from China's Huai River policy, P. Natl. Acad. Sci. USA, 110, 12936–12941, 2013.
Chipperfield, M.: New version of the TOMCAT/SLIMCAT off-line chemical transport model: intercomparison of stratospheric tracer experiments, Q. J. Roy. Meteor. Soc., 132, 1179–1203, 2006.

ACPD
15, 20449–20520, 2015

Cohen, A. J., Anderson, H. R., Ostro, B., Pandey, K. D., Krzyzanowski, M., Künzli, N., Gutschmidt, K., Pope III, C. A., Romieu, I., and Samet, J. M.: Urban air pollution, Comparative Quantification of Health Risks, 2, 1353–1433, 2004.

Cohen, A. J., Anderson, H. R., Ostro, B., Pandey, K. D., Krzyzanowski, M., Künzli, N., Gutschmidt, K., Pope III, C. A., Romieu, I., and Samet, J. M.: The global burden of disease due to outdoor air pollution, J. Toxicol. Env. Heal. A, 68, 1301–1307, 2005.

Cui, H., Mao, P., Zhao, Y., Nielsen, C. P., and Zhang, J.: Patterns in atmospheric carbonaceous aerosols in China: emission estimates and observed concentrations, Atmos. Chem. Phys. Discuss., 15, 8983–9032, doi:10.5194/acpd-15-8983-2015, 2015.

Denier van der Gon, H. A. C., Bergström, R., Fountoukis, C., Johansson, C., Pandis, S. N., Simpson, D., and Visschedijk, A. J. H.: Particulate emissions from residential wood combustion in Europe – revised estimates and an evaluation, Atmos. Chem. Phys., 15, 6503–6519, doi:10.5194/acp-15-6503-2015, 2015.

Dentener, F., Kinne, S., Bond, T., Boucher, O., Cofala, J., Generoso, S., Ginoux, P., Gong, S., Hoelzemann, J. J., Ito, A., Marelli, L., Penner, J. E., Putaud, J.-P., Textor, C., Schulz, M., van der Werf, G. R., and Wilson, J.: Emissions of primary aerosol and precursor gases in the years 2000 and 1750 prescribed data-sets for AeroCom, Atmos. Chem. Phys., 6, 4321–4344, doi:10.5194/acp-6-4321-2006, 2006.

Dusek, U., Frank, G., Hildebrandt, L., Curtius, J., Schneider, J., Walter, S., Chand, D., Drewnick, F., Hings, S., and Jung, D.: Size matters more than chemistry for cloud-nucleating ability of aerosol particles, Science, 312, 1375–1378, 2006.

Edwards, J. and Slingo, A.: Studies with a flexible new radiation code. I: Choosing a configuration for a large-scale model, Q. J. Roy. Meteor. Soc., 122, 689–719, 1996.

EEA: European Union emission inventory report, 1990–2012 under the UNECE Convention on Long-range Transboundary Air Pollution (LRTAP), EEA (European Environment Agency), Copenhagen, 2014.

Evan, A. T., Kossin, J. P., and Ramanathan, V.: Arabian Sea tropical cyclones intensified by emissions of black carbon and other aerosols, Nature, 479, 94–97, 2011.

Forster, P., Ramaswamy, V., Artaxo, P., Berntsen, T., Betts, R., Fahey, D. W., Haywood, J., Lean, J., Lowe, D. C., Myhre, G., Nganga, J., Prinn, R., Raga, G., Schulz, M., and Dorland, R. V.: Changes in Atmospheric Constituents and in Radiative Forcing, in: Climate Change 2007: The Physical Science Basis, Contribution of Working Group I to the Fourth Assessment Report of the Intergovernmental Panel on Climate Change, edited by: Solomon, S., Qin, D.,

ACPD
15, 20449–20520, 2015

Manning, M., Chen, Z., Marquis, M., Averyt, K. B., Tignor, M., and Miller, H. L., Cambridge University Press, Cambridge, UK, and New York, USA, 2007.
Fountoukis, C. and Nenes, A.: Continued development of a cloud droplet formation parameterization for global climate models, J. Geophys. Res.-Atmos., 110, D11212, doi:10.1029/2004jd005591, 2005.
Fountoukis, C., Butler, T., Lawrence, M., van der Gon, H. D., Visschedijk, A., Charalampidis, P., Pilinis, C., and Pandis, S.: Impacts of controlling biomass burning emissions on wintertime carbonaceous aerosol in Europe, Atmos. Environ., 87, 175–182, 2014.
Fu, T.-M., Cao, J. J., Zhang, X. Y., Lee, S. C., Zhang, Q., Han, Y. M., Qu, W. J., Han, Z., Zhang, R., Wang, Y. X., Chen, D., and Henze, D. K.: Carbonaceous aerosols in China: top-down constraints on primary sources and estimation of secondary contribution, Atmos. Chem. Phys., 12, 2725–2746, doi:10.5194/acp-12-2725-2012, 2012.
Fuller, K. A., Malm, W. C., and Kreidenweis, S. M.: Effects of mixing on extinction by carbonaceous particles, J. Geophys. Res.-Atmos., 104, 15941–15954, 1999.
Ganguly, D., Ginoux, P., Ramaswamy, V., Winker, D., Holben, B., and Tripathi, S.: Retrieving the composition and concentration of aerosols over the Indo-Gangetic basin using CALIOP and AERONET data, Geophys. Res. Lett., 36, L13806, doi:10.1029/2009GL038315, 2009.
Giannadaki, D., Pozzer, A., and Lelieveld, J.: Modeled global effects of airborne desert dust on air quality and premature mortality, Atmos. Chem. Phys., 14, 957–968, doi:10.5194/acp-14-957-2014, 2014.
Gong, S.: A parameterization of sea-salt aerosol source function for sub- and super-micron particles, Global Biogeochem. Cy., 17, 1097, doi:10.1029/2003gb002079, 2003.
Granier, C., Bessagnet, B., Bond, T., D'Angiola, A., Van Der Gon, H. D., Frost, G. J., Heil, A., Kaiser, J. W., Kinne, S., and Klimont, Z.: Evolution of anthropogenic and biomass burning emissions of air pollutants at global and regional scales during the 1980–2010 period, Climatic Change, 109, 163–190, 2011.
Guenther, A., Hewitt, C. N., Erickson, D., Fall, R., Geron, C., Graedel, T., Harley, P., Klinger, L., Lerdau, M., McKay, W. A., Pierce, T., Scholes, B., Steinbrecher, R., Tallamraju, R., Taylor, J., and Zimmerman, P.: A global model of natural volatile organic compound emissions, J. Geophys. Res., 100, 8873–8892, doi:10.1029/94jd02950, 1995.
Gustafsson, Ö., Kruså, M., Zencak, Z., Sheesley, R. J., Granat, L., Engström, E., Praveen, P., Rao, P., Leck, C., and Rodhe, H.: Brown clouds over South Asia: biomass or fossil fuel combustion?, Science, 323, 495–498, 2009.

ACPD
15, 20449–20520, 2015

Halmer, M. M., Schmincke, H. U., and Graf, H. F.: The annual volcanic gas input into the atmosphere, in particular into the stratosphere: a global data set for the past 100 years, J. Volcanol. Geoth. Res., 115, 511–528, doi:10.1016/s0377-0273(01)00318-3, 2002.

Han, Z., Zhang, R., Wang, Q. g., Wang, W., Cao, J., and Xu, J.: Regional modeling of organic aerosols over China in summertime, J. Geophys. Res.-Atmos., 113, D11202, doi:10.1029/2007JD009436, 2008.

Jacobson, M. Z.: Strong radiative heating due to the mixing state of black carbon in atmospheric aerosols, Nature, 409, 695–697, 2001.

Jacobson, M. Z.: Short-term effects of controlling fossil-fuel soot, biofuel soot and gases, and methane on climate, Arctic ice, and air pollution health, J. Geophys. Res.-Atmos., 115, D14209, doi:10.1029/2009JD013795, 2010.

Johnson, M., Edwards, R., Alatorre Frenk, C., and Masera, O.: In-field greenhouse gas emissions from cookstoves in rural Mexican households, Atmos. Environ., 42, 1206–1222, 2008.

Johnston, F. H., Henderson, S. B., Chen, Y., Randerson, J. T., Marlier, M., DeFries, R. S., Kinney, P., Bowman, D. M., and Brauer, M.: Estimated global mortality attributable to smoke from landscape fires, Environ. Health Persp., 120, 695–701, 2012.

Johnston, F. H., Hanigan, I. C., Henderson, S. B., and Morgan, G. G.: Evaluation of interventions to reduce air pollution from biomass smoke on mortality in Launceston, Australia: retrospective analysis of daily mortality, 1994–2007, Brit. Med. J., 346, e8446, doi:10.1136/bmj.e8446, 2013.

Kettle, A. and Andreae, M.: Flux of dimethylsulfide from the oceans: a comparison of updated data sets and flux models, J. Geophys. Res.-Atmos., 105, 26793–26808, 2000.

Kirchstetter, T. W., Novakov, T., and Hobbs, P. V.: Evidence that the spectral dependence of light absorption by aerosols is affected by organic carbon, J. Geophys. Res.-Atmos., 109, D21208, doi:10.1029/2004JD004999, 2004.

Kirillova, E. N., Andersson, A., Sheesley, R. J., Kruså, M., Praveen, P., Budhavant, K., Safai, P., Rao, P., and Gustafsson, Ö.: 13C-and, 14C-based study of sources and atmospheric processing of water-soluble organic carbon (WSOC) in South Asian aerosols, J. Geophys. Res.-Atmos., 118, 614–626, 2013.

Klimont, Z., Cofala, J., Xing, J., Wei, W., Zhang, C., Wang, S., Kejun, J., Bhandari, P., Mathur, R., and Purohit, P.: Projections of SO_2, NO_x and carbonaceous aerosols emissions in Asia, Tellus B, 61, 602–617, 2009.

ACPD
15, 20449–20520, 2015

Koch, D. and Del Genio, A. D.: Black carbon semi-direct effects on cloud cover: review and synthesis, Atmos. Chem. Phys., 10, 7685–7696, doi:10.5194/acp-10-7685-2010, 2010.

Koch, D., Schulz, M., Kinne, S., McNaughton, C., Spackman, J. R., Balkanski, Y., Bauer, S., Berntsen, T., Bond, T. C., Boucher, O., Chin, M., Clarke, A., De Luca, N., Dentener, F., Diehl, T., Dubovik, O., Easter, R., Fahey, D. W., Feichter, J., Fillmore, D., Freitag, S., Ghan, S., Ginoux, P., Gong, S., Horowitz, L., Iversen, T., Kirkevåg, A., Klimont, Z., Kondo, Y., Krol, M., Liu, X., Miller, R., Montanaro, V., Moteki, N., Myhre, G., Penner, J. E., Perlwitz, J., Pitari, G., Reddy, S., Sahu, L., Sakamoto, H., Schuster, G., Schwarz, J. P., Seland, Ø., Stier, P., Takegawa, N., Takemura, T., Textor, C., van Aardenne, J. A., and Zhao, Y.: Evaluation of black carbon estimations in global aerosol models, Atmos. Chem. Phys., 9, 9001–9026, doi:10.5194/acp-9-9001-2009, 2009.

Kulmala, M., Laaksonen, A., and Pirjola, L.: Parameterizations for sulfuric acid/water nucleation rates, J. Geophys. Res.-Atmos., 103, 8301–8307, 1998.

Kulmala, M., Lehtinen, K. E. J., and Laaksonen, A.: Cluster activation theory as an explanation of the linear dependence between formation rate of 3nm particles and sulphuric acid concentration, Atmos. Chem. Phys., 6, 787–793, doi:10.5194/acp-6-787-2006, 2006.

Kumar, R., Barth, M. C., Nair, V. S., Pfister, G. G., Suresh Babu, S., Satheesh, S. K., Krishna Moorthy, K., Carmichael, G. R., Lu, Z., and Streets, D. G.: Sources of black carbon aerosols in South Asia and surrounding regions during the Integrated Campaign for Aerosols, Gases and Radiation Budget (ICARB), Atmos. Chem. Phys., 15, 5415–5428, doi:10.5194/acp-15-5415-2015, 2015.

Lam, N. L., Chen, Y., Weyant, C., Venkataraman, C., Sadavarte, P., Johnson, M. A., Smith, K. R., Brem, B. T., Arineitwe, J., and Ellis, J. E.: Household light makes global heat: high black carbon emissions from kerosene wick lamps, Environ. Sci. Technol., 46, 13531–13538, 2012.

Lamarque, J.-F., Bond, T. C., Eyring, V., Granier, C., Heil, A., Klimont, Z., Lee, D., Liousse, C., Mieville, A., Owen, B., Schultz, M. G., Shindell, D., Smith, S. J., Stehfest, E., Van Aardenne, J., Cooper, O. R., Kainuma, M., Mahowald, N., McConnell, J. R., Naik, V., Riahi, K., and van Vuuren, D. P.: Historical (1850–2000) gridded anthropogenic and biomass burning emissions of reactive gases and aerosols: methodology and application, Atmos. Chem. Phys., 10, 7017–7039, doi:10.5194/acp-10-7017-2010, 2010.

ACPD
15, 20449–20520, 2015

Lei, Y., Zhang, Q., He, K. B., and Streets, D. G.: Primary anthropogenic aerosol emission trends for China, 1990–2005, Atmos. Chem. Phys., 11, 931–954, doi:10.5194/acp-11-931-2011, 2011.

Li, X., Wang, S., Duan, L., Hao, J., and Nie, Y.: Carbonaceous aerosol emissions from household biofuel combustion in China, Environ. Sci. Technol., 43, 6076–6081, 2009.

Lim, S. S., Vos, T., Flaxman, A. D., et al.: A comparative risk assessment of burden of disease and injury attributable to 67 risk factors and risk factor clusters in, 21 regions, 1990–2010: a systematic analysis for the Global Burden of Disease Study 2010, Lancet, 380, 2224–2260, 2012.

Mann, G. W., Carslaw, K. S., Spracklen, D. V., Ridley, D. A., Manktelow, P. T., Chipperfield, M. P., Pickering, S. J., and Johnson, C. E.: Description and evaluation of GLOMAP-mode: a modal global aerosol microphysics model for the UKCA composition-climate model, Geosci. Model Dev., 3, 519–551, doi:10.5194/gmd-3-519-2010, 2010.

Marlier, M. E., DeFries, R. S., Voulgarakis, A., Kinney, P. L., Randerson, J. T., Shindell, D. T., Chen, Y., and Faluvegi, G.: El Nino and health risks from landscape fire emissions in southeast Asia, Nature Climate Change, 3, 131–136, 2013.

Mathers, C., Fat, D. M., and Boerma, J.: The Global Burden of Disease: 2004 Update, World Health Organization, Switzerland, 2008.

Menon, S., Koch, D., Beig, G., Sahu, S., Fasullo, J., and Orlikowski, D.: Black carbon aerosols and the third polar ice cap, Atmos. Chem. Phys., 10, 4559–4571, doi:10.5194/acp-10-4559-2010, 2010.

Merikanto, J., Spracklen, D. V., Pringle, K. J., and Carslaw, K. S.: Effects of boundary layer particle formation on cloud droplet number and changes in cloud albedo from 1850 to 2000, Atmos. Chem. Phys., 10, 695–705, doi:10.5194/acp-10-695-2010, 2010.

Moorthy, K. K., Beegum, S. N., Srivastava, N., Satheesh, S., Chin, M., Blond, N., Babu, S. S., and Singh, S.: Performance evaluation of chemistry transport models over India, Atmos. Environ., 71, 210–225, 2013.

Nair, V. S., Solmon, F., Giorgi, F., Mariotti, L., Babu, S. S., and Moorthy, K. K.: Simulation of South Asian aerosols for regional climate studies, J. Geophys. Res.-Atmos., 117, D04209, doi:10.1029/2011JD016711, 2012.

Nenes, A. and Seinfeld, J. H.: Parameterization of cloud droplet formation in global climate models, J. Geophys. Res.-Atmos., 108, 4415, doi:10.1029/2002JD002911, 2003.

ACPD
15, 20449–20520, 2015

Nightingale, P. D., Malin, G., Law, C. S., Watson, A. J., Liss, P. S., Liddicoat, M. I., Boutin, J., and Upstill-Goddard, R. C.: In situ evaluation of air–sea gas exchange parameterizations using novel conservative and volatile tracers, Global Biogeochem. Cy., 14, 373–387, 2000.

Ostro, B.: Outdoor Air Pollution, WHO Environmental Burden of Disease Series, Geneva, Switzerland, 5, 2004.

Pagels, J., Dutcher, D. D., Stolzenburg, M. R., McMurry, P. H., Gälli, M. E., and Gross, D. S.: Fine-particle emissions from solid biofuel combustion studied with single-particle mass spectrometry: identification of markers for organics, soot, and ash components, J. Geophys. Res.-Atmos., 118, 859–870, 2013.

Parashar, D., Gadi, R., Mandal, T., and Mitra, A.: Carbonaceous aerosol emissions from India, Atmos. Environ., 39, 7861–7871, 2005.

Park, R. J., Jacob, D. J., Palmer, P. I., Clarke, A. D., Weber, R. J., Zondlo, M. A., Eisele, F. L., Bandy, A. R., Thornton, D. C., and Sachse, G. W.: Export efficiency of black carbon aerosol in continental outflow: global implications, J. Geophys. Res.-Atmos., 110, D11205, doi:10.1029/2004JD005432, 2005.

Partanen, A. I., Laakso, A., Schmidt, A., Kokkola, H., Kuokkanen, T., Pietikäinen, J.-P., Kerminen, V.-M., Lehtinen, K. E. J., Laakso, L., and Korhonen, H.: Climate and air quality trade-offs in altering ship fuel sulfur content, Atmos. Chem. Phys., 13, 12059–12071, doi:10.5194/acp-13-12059-2013, 2013.

Penner, J. E., Andreae, M., Annegarn, H., Barrie, L., Feichter, J., Hegg, D., Jayaraman, A., Leaitch, R., Murphy, D., Nganga, J., and Pitari, G.: Aerosols, their Direct and Indirect Effects, in: Climate Change 2001: The Physical Science Basis. Contribution of Working Group I to the Third Assessment Report of the Intergovernmental Panel on Climate Change, edited by: Houghton, J. T., Ding, Y., Griggs, D. J., Noguer, M., van der Linden, P. J., Dai, X., Maskell, K., and Johnson, C. A., Cambridge University Press, Cambridge, UK, and New York, USA, 2001.

Pierce, J. R. and Adams, P. J.: Uncertainty in global CCN concentrations from uncertain aerosol nucleation and primary emission rates, Atmos. Chem. Phys., 9, 1339–1356, doi:10.5194/acp-9-1339-2009, 2009.

Pierce, J. R., Chen, K., and Adams, P. J.: Contribution of primary carbonaceous aerosol to cloud condensation nuclei: processes and uncertainties evaluated with a global aerosol microphysics model, Atmos. Chem. Phys., 7, 5447–5466, doi:10.5194/acp-7-5447-2007, 2007.

ACPD
15, 20449–20520, 2015

Pierce, J., Theodoritsi, G., Adams, P., and Pandis, S.: Parameterization of the effect of sub-grid scale aerosol dynamics on aerosol number emission rates, J. Aerosol Sci., 40, 385–393, 2009.
Pope III, C. A. and Dockery, D. W.: Health effects of fine particulate air pollution: lines that connect, JAPCA J. Air Waste Ma., 56, 709–742, 2006.
Pope III, C. A., Burnett, R. T., Thun, M. J., Calle, E. E., Krewski, D., Ito, K., and Thurston, G. D.: Lung cancer, cardiopulmonary mortality, and long-term exposure to fine particulate air pollution, Jama, 287, 1132–1141, 2002.
Pringle, K. J., Carslaw, K. S., Spracklen, D. V., Mann, G. M., and Chipperfield, M. P.: The relationship between aerosol and cloud drop number concentrations in a global aerosol microphysics model, Atmos. Chem. Phys., 9, 4131–4144, doi:10.5194/acp-9-4131-2009, 2009.
Pringle, K. J., Carslaw, K. S., Fan, T., Mann, G.W., Hill, A., Stier, P., Zhang, K., and Tost, H.: A multi-model assessment of the impact of sea spray geoengineering on cloud droplet number, Atmos. Chem. Phys., 12, 11647–11663, doi:10.5194/acp-12-11647-2012, 2012.
Qu, W. J., Zhang, X. Y., Arimoto, R., Wang, D., Wang, Y. Q., Yan, L. W., and Li, Y.: Chemical composition of the background aerosol at two sites in southwestern and northwestern China: potential influences of regional transport, Tellus B, 60, 657–673, 2008.
Ramanathan, V. and Carmichael, G.: Global and regional climate changes due to black carbon, Nat. Geosci., 1, 221–227, 2008.
Ramanathan, V., Chung, C., Kim, D., Bettge, T., Buja, L., Kiehl, J., Washington, W., Fu, Q., Sikka, D., and Wild, M.: Atmospheric brown clouds: impacts on South Asian climate and hydrological cycle, P. Natl. Acad. Sci. USA, 102, 5326–5333, 2005.
Rap, A., Scott, C. E., Spracklen, D. V., Bellouin, N., Forster, P. M., Carslaw, K. S., Schmidt, A., and Mann, G.: Natural aerosol direct and indirect radiative effects, Geophys. Res. Lett., 40, 3297–3301, 2013.
Reddington, C. L., Carslaw, K. S., Spracklen, D. V., Frontoso, M. G., Collins, L., Merikanto, J., Minikin, A., Hamburger, T., Coe, H., Kulmala, M., Aalto, P., Flentje, H., Plass-Dülmer, C., Birmili, W., Wiedensohler, A., Wehner, B., Tuch, T., Sonntag, A., O'Dowd, C. D., Jennings, S. G., Dupuy, R., Baltensperger, U., Weingartner, E., Hansson, H.-C., Tunved, P., Laj, P., Sellegri, K., Boulon, J., Putaud, J.-P., Gruening, C., Swietlicki, E., Roldin, P., Henzing, J. S., Moerman, M., Mihalopoulos, N., Kouvarakis, G., Ždímal, V., Zíková, N., Marinoni, A., Bonasoni, P., and Duchi, R.: Primary versus secondary contributions to particle number concentrations in

ACPD
15, 20449–20520, 2015

the European boundary layer, Atmos. Chem. Phys., 11, 12007–12036, doi:10.5194/acp-11-12007-2011, 2011.
Roden, C. A., Bond, T. C., Conway, S., and Pinel, A. B. O.: Emission factors and real-time optical properties of particles emitted from traditional wood burning cookstoves, Environ. Sci. Technol., 40, 6750–6757, 2006.
Roden, C. A., Bond, T. C., Conway, S., Osorto Pinel, A. B., MacCarty, N., and Still, D.: Laboratory and field investigations of particulate and carbon monoxide emissions from traditional and improved cookstoves, Atmos. Environ., 43, 1170–1181, 2009.
Rossow, W. B. and Schiffer, R. A.: Advances in understanding clouds from ISCCP, B. Am. Meteorol. Soc., 80, 2261–2287, 1999.
Schlesinger, R., Kunzli, N., Hidy, G., Gotschi, T., and Jerrett, M.: The health relevance of ambient particulate matter characteristics: coherence of toxicological and epidemiological inferences, Inhal. Toxicol., 18, 95–125, 2006.
Schmidt, A., Ostro, B., Carslaw, K. S., Wilson, M., Thordarson, T., Mann, G. W., and Simmons, A. J.: Excess mortality in Europe following a future Laki-style Icelandic eruption, P. Natl. Acad. Sci. USA, 108, 15710–15715, 2011.
Schmidt, A., Carslaw, K. S., Mann, G. W., Rap, A., Pringle, K. J., Spracklen, D. V., Wilson, M., and Forster, P. M.: Importance of tropospheric volcanic aerosol for indirect radiative forcing of climate, Atmos. Chem. Phys., 12, 7321–7339, doi:10.5194/acp-12-7321-2012, 2012.
Scott, C. E., Rap, A., Spracklen, D. V., Forster, P. M., Carslaw, K. S., Mann, G. W., Pringle, K. J., Kivekäs, N., Kulmala, M., Lihavainen, H., and Tunved, P.: The direct and indirect radiative effects of biogenic secondary organic aerosol, Atmos. Chem. Phys., 14, 447–470, doi:10.5194/acp-14-447-2014, 2014.
SEDAC: Sociodemographic Data and Applications Centre, Gridded Population of the World (GPW), v3., available at: http://sedac.ciesin.columbia.edu/data/collection/gpw-v3(last acces: 1 November 2013), 2004.
Sheesley, R. J., Kirillova, E., Andersson, A., Kruså, M., Praveen, P., Budhavant, K., Safai, P. D., Rao, P., and Gustafsson, Ö.: Year-round radiocarbon-based source apportionment of carbonaceous aerosols at two background sites in South Asia. J. Geophys. Res.-Atmos., 117, D10202, doi:10.1029/2011JD017161, 2012.
Shen, G., Wang, W., Yang, Y., Zhu, C., Min, Y., Xue, M., Ding, J., Li, W., Wang, B., and Shen, H.: Emission factors and particulate matter size distribution of polycyclic aromatic hydrocarbons

ACPD
15, 20449–20520, 2015

from residential coal combustions in rural Northern China, Atmos. Environ., 44, 5237–5243, 2010.
Sihto, S.-L., Kulmala, M., Kerminen, V.-M., Dal Maso, M., Petäjä, T., Riipinen, I., Korhonen, H., Arnold, F., Janson, R., Boy, M., Laaksonen, A., and Lehtinen, K. E. J.: Atmospheric sulphuric acid and aerosol formation: implications from atmospheric measurements for nucleation and early growth mechanisms, Atmos. Chem. Phys., 6, 4079–4091, doi:10.5194/acp-6-4079-2006, 2006.
Silva, R. A., West, J. J., Zhang, Y., Anenberg, S. C., Lamarque, J.-F., Shindell, D. T., Collins, W. J., Dalsoren, S., Faluvegi, G., and Folberth, G.: Global premature mortality due to anthropogenic outdoor air pollution and the contribution of past climate change, Environ. Res. Lett., 8, 034005, doi:10.1088/1748-9326/8/3/034005, 2013.
Smith, K. R., Bruce, N., Balakrishnan, K., Adair-Rohani, H., Balmes, J., Chafe, Z., Dherani, M., Hosgood, H. D., Mehta, S., and Pope, D.: Millions dead: how do we know and what does it mean? Methods used in the comparative risk assessment of household air pollution, Annu. Rev. Publ. Health, 35, 185–206, 2014.
Spracklen, D. V., Pringle, K. J., Carslaw, K. S., Chipperfield, M. P., and Mann, G. W.: A global off-line model of size-resolved aerosol microphysics: I. Model development and prediction of aerosol properties, Atmos. Chem. Phys., 5, 2227–2252, doi:10.5194/acp-5-2227-2005, 2005a.
Spracklen, D. V., Pringle, K. J., Carslaw, K. S., Chipperfield, M. P., and Mann, G. W.: A global off-line model of size-resolved aerosol microphysics: II. Identification of key uncertainties, Atmos. Chem. Phys., 5, 3233–3250, doi:10.5194/acp-5-3233-2005, 2005b.
Spracklen, D. V., Carslaw, K. S., Pöschl, U., Rap, A., and Forster, P. M.: Global cloud condensation nuclei influenced by carbonaceous combustion aerosol, Atmos. Chem. Phys., 11, 9067–9087, doi:10.5194/acp-11-9067-2011, 2011a.
Spracklen, D. V., Jimenez, J. L., Carslaw, K. S., Worsnop, D. R., Evans, M. J., Mann, G. W., Zhang, Q., Canagaratna, M. R., Allan, J., Coe, H., McFiggans, G., Rap, A., and Forster, P.: Aerosol mass spectrometer constraint on the global secondary organic aerosol budget, Atmos. Chem. Phys., 11, 12109–12136, doi:10.5194/acp-11-12109-2011, 2011b.
Stier, P., Feichter, J., Kinne, S., Kloster, S., Vignati, E., Wilson, J., Ganzeveld, L., Tegen, I., Werner, M., Balkanski, Y., Schulz, M., Boucher, O., Minikin, A., and Petzold, A.: The aerosol-climate model ECHAM5-HAM, Atmos. Chem. Phys., 5, 1125–1156, doi:10.5194/acp-5-1125-2005, 2005.

ACPD
15, 20449–20520, 2015

Stohl, A., Klimont, Z., Eckhardt, S., Kupiainen, K., Shevchenko, V. P., Kopeikin, V. M., and Novigatsky, A. N.: Black carbon in the Arctic: the underestimated role of gas flaring and residential combustion emissions, Atmos. Chem. Phys., 13, 8833–8855, doi:10.5194/acp-13-8833-2013, 2013.

Stone, E. A., Lough, G. C., Schauer, J. J., Praveen, P., Corrigan, C., and Ramanathan, V.: Understanding the origin of black carbon in the atmospheric brown cloud over the Indian Ocean. J. Geophys. Res.-Atmos., 112, D22S23, doi:10.1029/2006JD008118, 2007.

Stone, E. A., Schauer, J. J., Pradhan, B. B., Dangol, P. M., Habib, G., Venkataraman, C., and Ramanathan, V.: Characterization of emissions from South Asian biofuels and application to source apportionment of carbonaceous aerosol in the Himalayas. J. Geophys. Res.-Atmos., 115, D06301, doi:10.1029/2009JD011881, 2010.

Stone, E. A., Yoon, S.-C., and Schauer, J. J.: Chemical characterization of fine and coarse particles in Gosan, Korea during springtime dust events, Aerosol Air Qual. Res., 11, 31–43, 2011.

Tiitta, P., Vakkari, V., Croteau, P., Beukes, J. P., van Zyl, P. G., Josipovic, M., Venter, A. D., Jaars, K., Pienaar, J. J., Ng, N. L., Canagaratna, M. R., Jayne, J. T., Kerminen, V.-M., Kokkola, H., Kulmala, M., Laaksonen, A., Worsnop, D. R., and Laakso, L.: Chemical composition, main sources and temporal variability of PM_1 aerosols in southern African grassland, Atmos. Chem. Phys., 14, 1909–1927, doi:10.5194/acp-14-1909-2014, 2014.

Tsigaridis, K., Daskalakis, N., Kanakidou, M., Adams, P. J., Artaxo, P., Bahadur, R., Balkanski, Y., Bauer, S. E., Bellouin, N., Benedetti, A., Bergman, T., Berntsen, T. K., Beukes, J. P., Bian, H., Carslaw, K. S., Chin, M., Curci, G., Diehl, T., Easter, R. C., Ghan, S. J., Gong, S. L., Hodzic, A., Hoyle, C. R., Iversen, T., Jathar, S., Jimenez, J. L., Kaiser, J. W., Kirkevåg, A., Koch, D., Kokkola, H., Lee, Y. H, Lin, G., Liu, X., Luo, G., Ma, X., Mann, G. W., Mihalopoulos, N., Morcrette, J.-J., Müller, J.-F., Myhre, G., Myriokefalitakis, S., Ng, N. L., O'Donnell, D., Penner, J. E., Pozzoli, L., Pringle, K. J., Russell, L. M., Schulz, M., Sciare, J., Seland, Ø., Shindell, D. T., Sillman, S., Skeie, R. B., Spracklen, D., Stavrakou, T., Steenrod, S. D., Takemura, T., Tiitta, P., Tilmes, S., Tost, H., van Noije, T., van Zyl, P. G., von Salzen, K., Yu, F., Wang, Z., Wang, Z., Zaveri, R. A., Zhang, H., Zhang, K., Zhang, Q., and Zhang, X.: The AeroCom evaluation and intercomparison of organic aerosol in global models, Atmos. Chem. Phys., 14, 10845–10895, doi:10.5194/acp-14-10845-2014, 2014.

ACPD
15, 20449–20520, 2015

UNEP: Near-term Climate Protection and Clean Air Benefits: Actions for Controlling Short-Lived Climate Forcers, United Nations Environment Programme (UNEP), Nairobi, Kenya, 78 pp., 2011.

Unger, N., Bond, T. C., Wang, J. S., Koch, D. M., Menon, S., Shindell, D. T., and Bauer, S.: Attribution of climate forcing to economic sectors, P. Natl. Acad. Sci. USA, 107, 3382–3387, 2010.

Vakkari, V., Beukes, J. P., Laakso, H., Mabaso, D., Pienaar, J. J., Kulmala, M., and Laakso, L.: Long-term observations of aerosol size distributions in semi-clean and polluted savannah in South Africa, Atmos. Chem. Phys., 13, 1751–1770, doi:10.5194/acp-13-1751-2013, 2013.

van der Werf, G. R., Randerson, J. T., Collatz, G. J., Giglio, L., Kasibhatla, P. S., Arellano, A. F., Olsen, S. C., and Kasischke, E. S.: Continental-scale partitioning of fire emissions during the 1997 to 2001 El Nino/La Nina period, Science, 303, 73–76, 2004.

Venkataraman, C. and Rao, G. U. M.: Emission factors of carbon monoxide and size-resolved aerosols from biofuel combustion, Environ. Sci. Technol., 35, 2100–2107, 2001.

Venkataraman, C., Habib, G., Eiguren-Fernandez, A., Miguel, A., and Friedlander, S.: Residential biofuels in South Asia: carbonaceous aerosol emissions and climate impacts, Science, 307, 1454–1456, 2005.

Venter, A. D., Vakkari, V., Beukes, J. P., Van Zyl, P. G., Laakso, H., Mabaso, D., Tiitta, P., Josipovic, M., Kulmala, M., and Pienaar, J. J.: An air quality assessment in the industrialised western Bushveld Igneous Complex, South Africa, S. Afr. J. Sci., 108, 1–10, 2012.

Wang, R., Tao, S., Balkanski, Y., Ciais, P., Boucher, O., Liu, J., Piao, S., Shen, H., Vuolo, M. R., and Valari, M.: Exposure to ambient black carbon derived from a unique inventory and high-resolution model, P. Natl. Acad. Sci. USA, 111, 2459–2463, 2014.

Wang, X., Wang, Y., Hao, J., Kondo, Y., Irwin, M., Munger, J. W., and Zhao, Y.: Top-down estimate of China's black carbon emissions using surface observations: sensitivity to observation representativeness and transport model error, J. Geophys. Res.-Atmos., 118, 5781–5795, 2013.

Wang, X., Heald, C. L., Ridley, D. A., Schwarz, J. P., Spackman, J. R., Perring, A. E., Coe, H., Liu, D., and Clarke, A. D.: Exploiting simultaneous observational constraints on mass and absorption to estimate the global direct radiative forcing of black carbon and brown carbon, Atmos. Chem. Phys., 14, 10989–11010, doi:10.5194/acp-14-10989-2014, 2014.

WHO: The Energy Access Situation in Developing Countries, World Health Organization and United Nations Development Programme, New York, USA, 2009.

ACPD
15, 20449–20520, 2015

WHO: Burden of Disease from Household Air Pollution for 2012, World Health Organisation, Geneva, Switzerland, 2014a.

WHO: Burden of Disease from Ambient Air pollution for 2012, World Health Organisation, Geneva, Switzerland, 2014b.

Xu, B., Cao, J., Hansen, J., Yao, T., Joswia, D. R., Wang, N., Wu, G., Wang, M., Zhao, H., and Yang, W.: Black soot and the survival of Tibetan glaciers, P. Natl. Acad. Sci. USA, 106, 22114–22118, 2009.

Yu, S., Eder, B., Dennis, R., Chu, S. H., and Schwartz, S. E.: New unbiased symmetric metrics for evaluation of air quality models, Atmos. Sci. Lett., 7, 26–34, 2006.

Zhang, X., Wang, Y., Zhang, X., Guo, W., and Gong, S.: Carbonaceous aerosol composition over various regions of China during 2006, J. Geophys. Res.-Atmos., 113, D14111, doi:10.1029/2007JD009525, 2008.

Zhi, G., Chen, Y., Feng, Y., Xiong, S., Li, J., Zhang, G., Sheng, G., and Fu, J.: Emission characteristics of carbonaceous particles from various residential coal-stoves in China, Environ. Sci. Technol., 42, 3310–3315, 2008.

ACPD

15, 20449–20520, 2015

Table 1. Acronyms used in this study.

Acronym	Description
ACCMIP	Atmospheric Chemistry and Climate Model Intercomparison Project
AF	Attributable fraction
AIE	Aerosol indirect effect
BC	Black carbon
BHN	Binary homogenous nucleation
BLN	Boundary layer nucleation
CCN	Cloud condensation nuclei
CDNC	Cloud droplet number concentration
CPD	Cardiopulmonary disease
CRF	Concentration response functions
DRE	Direct radiative effect
EC	Elemental carbon
FT	Free troposphere
LC	Lung Cancer
LPG	Liquefied petroleum gas
LW	Longwave
MACCity	MACC/CityZEN project
N_3	Number of particles greater than 3 nm dry diameter
N_{50}	Number of particles greater than 50 nm dry diameter
N_{100}	Number of particles greater than 100 nm dry diameter
NMBF	Normalised mean bias factor
OC	Organic carbon
PM	Particulate matter
$PM_{2.5}$	Particulate matter with an aerodynamic dry diameter of $< 2.5\,\mu m$
POM	Particulate organic matter
RE	Radiative effect
RR	Relative risk
RSF	Residential solid fuel
SOA	Secondary organic aerosol
SW	Shortwave
TOA	Top-of-atmosphere

ACPD
15, 20449–20520, 2015

Table 2. Summary of aerosol observations used in this study.

Site name	Site description	Measurement	Measurement period	Measurement technique	Reference
Eastern European sites					
Kosetice (49.34° N, 15.4° E)	Rural site in Central Czech Republic	EC and OC in size fraction $PM_{2.5}$	2010	EC and OC: thermal-optically	*
Iskrba (45.34° N, 14.52° E)	Rural site in Southern Slovenia	EC and OC in size fraction $PM_{2.5}$	2010	EC and OC: thermal-optically	*
Southern African sites					
Botsalano (25.54° S, 25.75° E)	Rural site in North Eastern South Africa	$PM_{2.5}$ mass and aerosol number distribution	2007	$PM_{2.5}$ mass: TEOM Monitor; aerosol number distribution: DMPS	Vakkari et al. (2013)
Marikana (25.70° S, 27.48° E)	Semi-urban site in North Eastern SouthAfrica	BC and aerosol number distribution	2008	BC: thermo model 5012 multiangle absorption photometer; aerosol number distribution: DMPS	Vakkari et al. (2013)
Welgegund (26.57° S, 26.94° E)	Semi-rural site in North Eastern South Africa	Aerosol number distribution	2011	Aerosol number distribution: DMPS	Tiitta et al. (2014)
South Asian sites					
Hanimaadho (6.87° N, 73.18° E)	Background site in Maldives	$PM_{2.5}$ mass, EC and OC in size fraction $PM_{2.5}$; aerosol number distribution and fossil and non-fossil BC and EC fractions	Oct–Jan 2004–2005; Jan–Jul 2005 See references for 14C analysis dates	$PM_{2.5}$: gravimetrically; EC and OC: thermal-optically; aerosol number distribution: SMPS ^{14}C analysis	Stone et al. (2007) Gustafsson et al. (2009) Sheesley et al. (2012) Bosch et al. (2014)
Godavari (27.59° N, 85.31° E)	Rural/near-urban site in the foothills of the Himalayas	EC and OC in size fraction $PM_{2.5}$	Jan–Dec 2006	EC and OC: thermal-optically	Stone et al. (2010)
Port Blair (11.6° N, 92.7° E)	Background site located on an island in Bay of Bengal	BC concentration	2006	BC: optically by aethalometer	Moorthy et al. (2013)
Minicoy (8.3° N, 73.0° E)	Background site located on an island in the Arabian Sea	BC concentration	2006	BC: optically by aethalometer	Moorthy et al. (2013)
Kharagpur (22.5° N, 87.5° E)	Semi-urban site in the Indo-Gangetic Plain	BC concentration	2006	BC: optically by aethalometer	Moorthy et al. (2013)
Trivandrum (8.55° N, 76.9° E)	Semi-urban coastal site in Southern India	BC concentration	2006	BC: optically by aethalometer	Moorthy et al. (2013)

ACPD
15, 20449–20520, 2015

Table 2. Continued.

Site name	Site description	Measurement	Measurement period	Measurement technique	Reference
East Asian sites					
Gosan (33.38° N, 126.25° E)	Background site on Jeju Island, South Korea	$PM_{2.5}$ mass, EC and OC in size fraction $PM_{2.5}$	Jan–Jul 2007	$PM_{2.5}$: gravimetrically; EC and OC: thermal-optically	Stone et al. (2011)
Akdala (47.1° N, 87.97° E)	Background site in North West China	EC and OC in size fraction PM_{10}	Aug, Sep, Nov, and Dec 2004; Jan–Mar 2005	EC and OC: thermal-optically	Qu et al. (2008)
Zhuzhang (28° N, 99.72° E)	Background site in Southern China	EC and OC in size fraction PM_{10}	Aug–Dec 2004; Jan–Feb 2005	EC and OC: thermal-optically	Qu et al. (2008)
Dunhuang (40.15° N, 94.68° E)	Rural site in North West China	EC and OC in size fraction PM_{10}	2006	EC and OC: thermal-optically	Zhang et al. (2008)
Gaolanshan (36° N, 105.85° E)	Rural site in Central China	EC and OC in size fraction PM_{10}	2006	EC and OC: thermal-optically	Zhang et al. (2008)
Wusumu (40.56° N, 112.55° E)	Rural site in North East China	EC and OC in size fraction PM_{10}	Sep 2005; Jan and Jul 2006; May 2007	EC and OC: thermal-optically	Han et al. (2008)
Longfengshan (44.73° N, 127.6° E)	Rural site in North East China	EC and OC in size fraction PM_{10}	2006	EC and OC: thermal-optically	Zhang et al. (2008)
Taiyangshan (29.17° N, 111.71° E)	Rural site in Central China.	EC and OC in size fraction PM_{10}	2006	EC and OC: thermal-optically	Zhang et al. (2008)
Jinsha (29.63° N, 114.2° E)	Rural site in Central China	EC and OC in size fraction PM_{10}	Jun–Nov 2006	EC and OC: thermal-optically	Zhang et al. (2008)
LinAn (30.3° N, 119.73° E)	Rural site in Eastern China	EC and OC in size fraction PM_{10}	2004–2005	EC and OC: thermal-optically	Zhang et al. (2008)

* Data obtained through the EBAS atmospheric database [http://ebas.nilu.no/Default.aspx].

ACPD
15, 20449–20520, 2015

Table 3. Summary of model simulations and global annual mean values and changes to BC and POM burden, continental surface $PM_{2.5}$, surface total particle number (N_3, diameter > 3 nm), N_{50} (diameter > 50 nm), low-cloud level (850–900 hPa) CDNC concentrations (0.15 and 0.3 ms^{-1} cloud updraft velocity over sea and land, respectively), and all-sky DRE and first AIE, relative to an equivalent experiment where residential emissions have been removed. We estimate annual global mortality for cardiopulmonary disease (CPD) and lung cancer (LC) following Ostro (2004) showing 95 % confidence interval (total in bold). Emissions used are either the ACCMIP dataset (A) or the MACCity dataset (M) with perturbations to residential emissions applied as detailed. For emitted carbonaceous size distributions, see Table footnote.

Expt. No.	Description	Emissions	BC burden (Tg)	POM burden (Tg)	$PM_{2.5}$ ($\mu g/m^3$)	N_3 (cm^{-3})	N_{50} (cm^{-3})	CDNC (cm^{-3})	Mortality ('000)	All-sky DRE ($mW\ m^{-2}$)	First AIE ($mW\ m^{-2}$)
1	**res_base_off**	None	–	–	–	–	–	–	–	–	–
2	**res_base** All annual mean anthropogenic emissions (including residential emissions)[a]	A	0.11 +0.024 (+25.68)	1.07 +0.135 (+14.33)	4.19 +0.08 (+2.01)	778.51 −7.99 (−1.01 %)	381.81 +17.20 (+4.72 %)	214.61 +4.41 (+2.10 %)	CPD: 289 (106–467) LC: 26 (10–41) Total: **315 (115–508)**	**-5**	**-25**
3	**res_aero** AeroCom recommended size distribution for residential primary carbonaceous particles[b]	A	0.12 +0.025 (+26.69)	1.08 +0.145 (+15.32)	4.19 +0.08 (+2.03)	807.77 +19.11 (+2.43 %)	396.99 +31.32 (+8.56 %)	216.59 +6.39 (+3.04 %)	CPD: 288 (106–46) LC: 26 (10–41) Total: **314 (116–507)**	**1**	**-46**
4	**res_small** Observed lower bound limit size distribution for residential primary carbonaceous particles[c]	A	0.12 +0.028 (+29.20)	1.19 +0.22 (+22.59)	4.21 +0.09 (+2.25)	2593.62 +1612.46 (+164.34)	689.74 +253.37 (+58.06 %)	252.68 +42.48 (+20.21 %)	CPD: 270 (98–435) LC: 24 (9–38) Total: **294 (108–473)**	**63**	**-502**
5	**res_large** Observed upper bound limit size distribution for residential primary carbonaceous particles[d]	A	0.11 +0.024 (+25.38 %)	1.07 +0.133 (+14.07 %)	4.19 +0.08 (+1.99 %)	768.03 −17.68 (−2.25 %)	375.94 +11.73 (+3.22 %)	213.85 +3.65 (+1.74 %)	CPD: 290 000 (106–468) LC: 26 (10–41) Total: **316 (116–509)**	**-7**	**-16**
6	**res_×2** Primary residential BC and POM doubled globally[a]	A, BC/OC× 2	0.14 +0.047 (+49.90 %)	1.20 +0.263 (+27.90 %)	4.25 +0.14 (+3.48 %)	776.73 −9.76 (−1.24 %)	387.52 +22.90 (+6.28 %)	215.82 +5.62 (+2.67 %)	CPD: 477 (177–764) LC: 42 (16–66) Total: **519 (193–830)**	**21**	**-25**

ACPD
15, 20449–20520, 2015

Table 3. Continued.

Expt. No.	Description	Emissions	BC burden (Tg)	POM burden (Tg)	$PM_{2.5}$ ($\mu g/m^3$)	N_3 (cm^{-3})	N_{50} (cm^{-3})	CDNC (cm^{-3})	Mortality ('000)	All-sky DRE ($mW\ m^{-2}$)	First AIE ($mW\ m^{-2}$)
7	**res_BC×2** Primary residential BC doubled globally[a]	A, BC×2	0.14 +0.051 (+53.81 %)	1.07 +0.134 (+14.21 %)	4.20 +0.06 (+2.24 %)	778.32 −8.18 (−1.04 %)	383.19 +18.58 (+5.09 %)	214.91 +4.71 (+2.24 %)	CPD: 320 (118–517) LC: 28 (11–46) Total: **348 (129–563)**	**85**	**-26**
8	**res_POM×2** Primary residential POM doubled globally[a]	A, OC×2	0.11 +0.022 (+23.06 %)	1.20 +0.264 (+28.01 %)	4.24 +0.14 (+3.25 %)	776.25 −10.25 (−1.30 %)	386.42 +21.81 (+5.98 %)	215.55 +5.35 (+2.55 %)	CPD: 433 (160–695) LC: 39 (15–62) Total: **472 (175–757)**	**-66**	**-23**
9	**res_SO2×2** Primary residential SO_2 doubled globally[a]	A, SO2×2	0.11 +0.024 (+25.19 %)	1.07 +0.122 (+14.11 %)	4.21 +0.06 (+2.52 %)	785.99 −0.51 (−0.06 %)	388.35 +23.74 (+6.51 %)	217.23 +7.03 (+3.34 %)	CPD: 306 (113–494) LC: 29 (11–46) Total: **336 (124–540)**	**-43**	**-45**
10	**res_BHN_off**	None	–	–	–	–	–	–	–	–	–
11	**res_BHN** Binary homogeneous nucleation only. Boundary layer activation nucleation switched off[a]	A	0.11 +0.023 (+25.46 %)	1.04 +0.131 (+14.33 %)	4.18 +0.08 (+2.01 %)	431.91 +23.41 (+5.73 %)	306.09 +18.73 (+6.52 %)	187.76 +5.7 (+3.13 %)	CPD: 289 (106–467) LC: 26 (10–41) Total: **315 (116–508 000)**	**-8**	**-52**
12	**res_monthly_off**	None	–	–	–	–	–	–	–	–	–
13	**res_monthly** Monthly varying anthropogenic emissions (including residential emissions) [a]	M	0.11 +0.024 (+25.38 %)	1.08 +0.135 (+14.37 %)	4.19 +0.08 (+2.07 %)	797.54 −12.23 (−1.51 %)	393.16 +18.17 (+4.84 %)	219.57 +5.09 (+2.37 %)	CPD: 283 (104–457) LC: 25 (9–40) Total: **308 (113–497)**	**-8**	**-20**
14	**res_monthly_× 2** Primary residential BC and POM doubled globally[a]	M, BC/OC× 2	0.14 +0.047 (+49.76 %)	1.20 +0.265 (+27.99 %)	0.25 +0.15 (+3.62 %)	794.68 −15.09 (−1.86 %)	399.03 +24.04 (+6.41 %)	220.47 +5.99 (+2.79 %)	CPD: 475 (176–761) LC: 41 (16–66) Total: **517 (192–827)**	**10**	**-21**

[a] Stier et al. (2005) recommended residential (biomass/biofuel) primary carbonaceous particle sizes, D = 150 nm σ = 1.59.
[b] AerCom recommended residential (biomass/biofuel) primary carbonaceous particle sizes, (Dentener et al., 2006), D = 80 nm σ = 1.8.
[c] Observed lower bound limit for RSF primary carbonaceous particle sizes, D = 20 nm σ = 1.8 (Bond et al., 2006).
[d] Observed lower bound limit for RSF primary carbonaceous particle sizes, D = 500 nm σ = 1.8 (Bond et al., 2006).

ACPD
15, 20449–20520, 2015

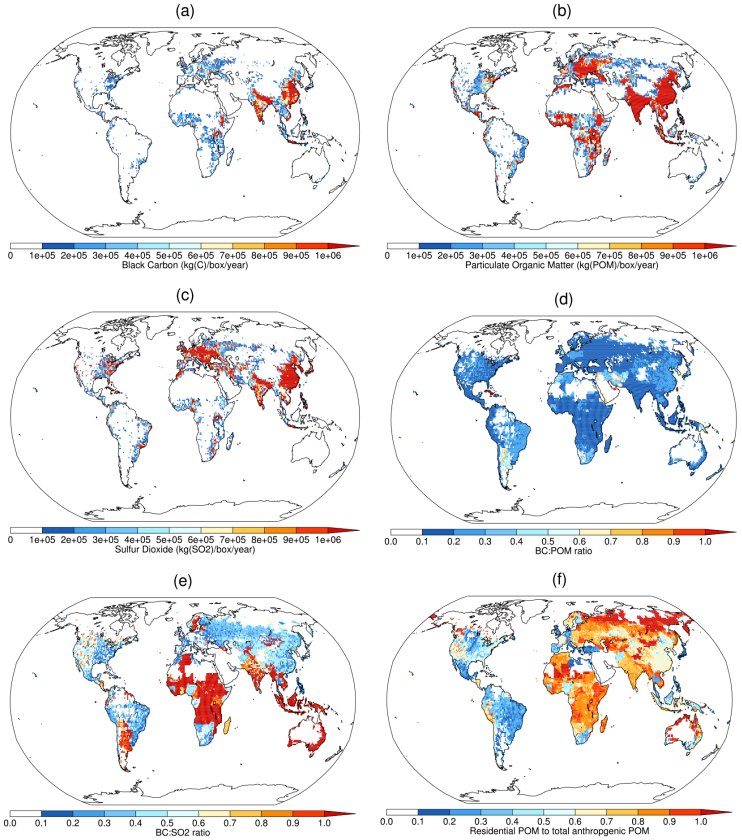

Figure 1. Annual residential emissions from the ACCMIP emission dataset for BC **(a)**, POM **(b)**, SO_2 **(c)**, BC : POM ratio **(d)**, BC : SO2 ratio **(e)** and residential POM to total anthropogenic POM **(f)**.

ACPD
15, 20449–20520, 2015

The impact of residential combustion emissions

E. W. Butt et al.

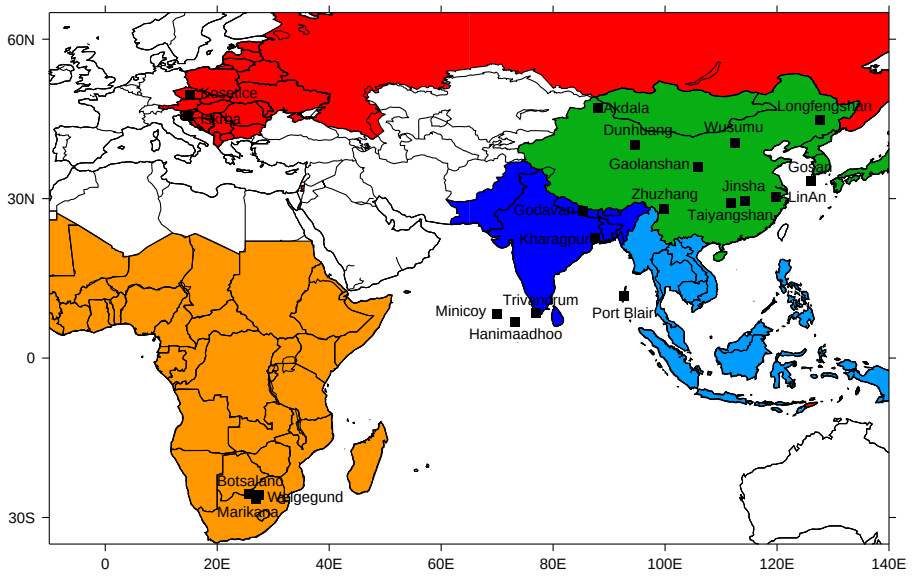

Figure 2. Locations of aerosol measurements used in this study and geographical regions of Eastern Europe and the Russian Federation (red), Africa (orange), South Asia (dark blue), Southeast Aisa (light blue) and East Asia (green).

ACPD
15, 20449–20520, 2015

The impact of residential combustion emissions

E. W. Butt et al.

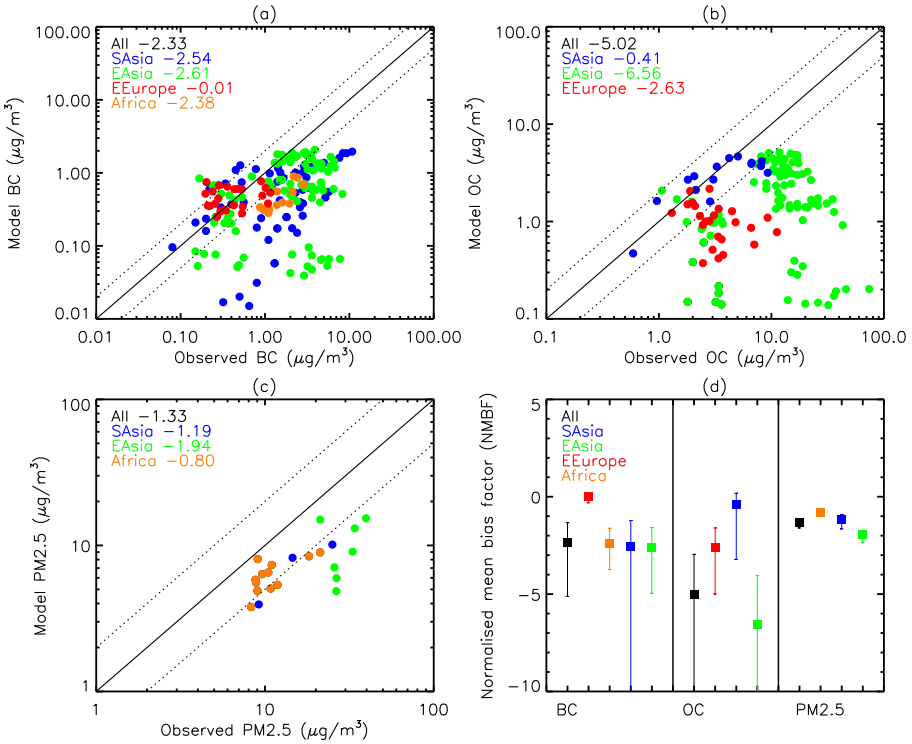

Figure 3. Observed and simulated BC **(a)**, OC **(b)** and $PM_{2.5}$ **(c)** concentrations for the baseline simulation (res_base) using ACCMIP emissions. **(d)** Normalised mean bias factor (NMBF) where square shows the baseline simulation, bottom error bar shows the range for removed residential emissions (res_base_off) and top error bar shows residential carbonaceous emissions doubled (res_×2). Colours represent locations within regions defined in Fig. 2: all locations (All: black), South Asia (SAsia: blue), East Asia (EAsia: green), Eastern Europe and the Russian Federation (EEurope: red) and Africa (Africa: orange).

ACPD
15, 20449–20520, 2015

The impact of residential combustion emissions

E. W. Butt et al.

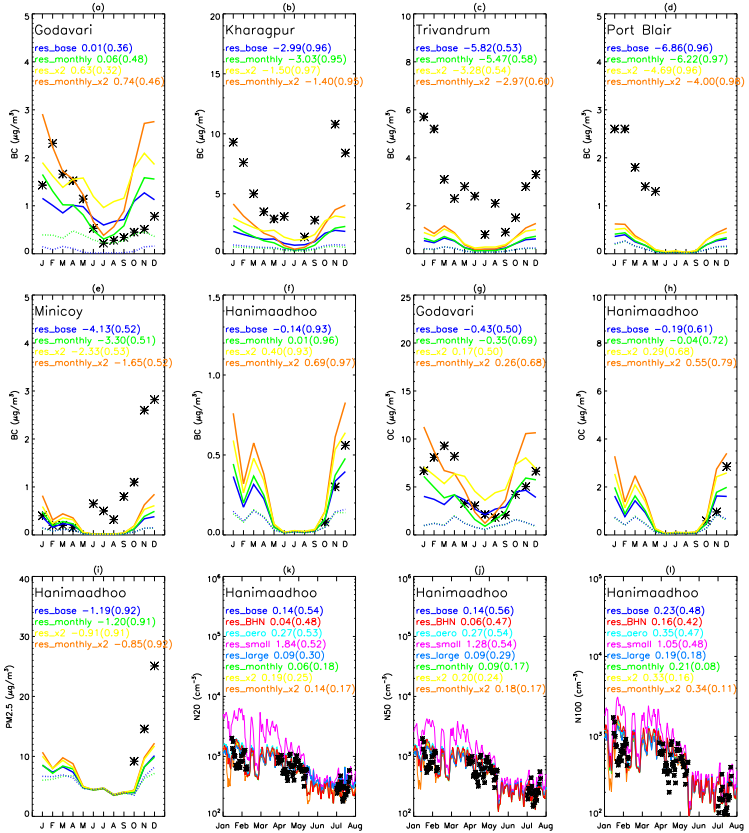

Figure 4. Observed (black stars) and simulated monthly mean BC **(a–f)**, OC **(g–h)**, $PM_{2.5}$ **(i)**, and daily mean N_{20} **(k)**, N_{50} **(j)**, and N_{100} **(l)** at South Asian locations. Normalised mean bias factor (NMBF) and correlation coefficient (r) are reported for each model simulation: NMBF(r). Experiments where residential emissions have been removed are represented by the blue (res_base_off) and green (res_monthly_off) dotted lines.

ACPD
15, 20449–20520, 2015

The impact of residential combustion emissions

E. W. Butt et al.

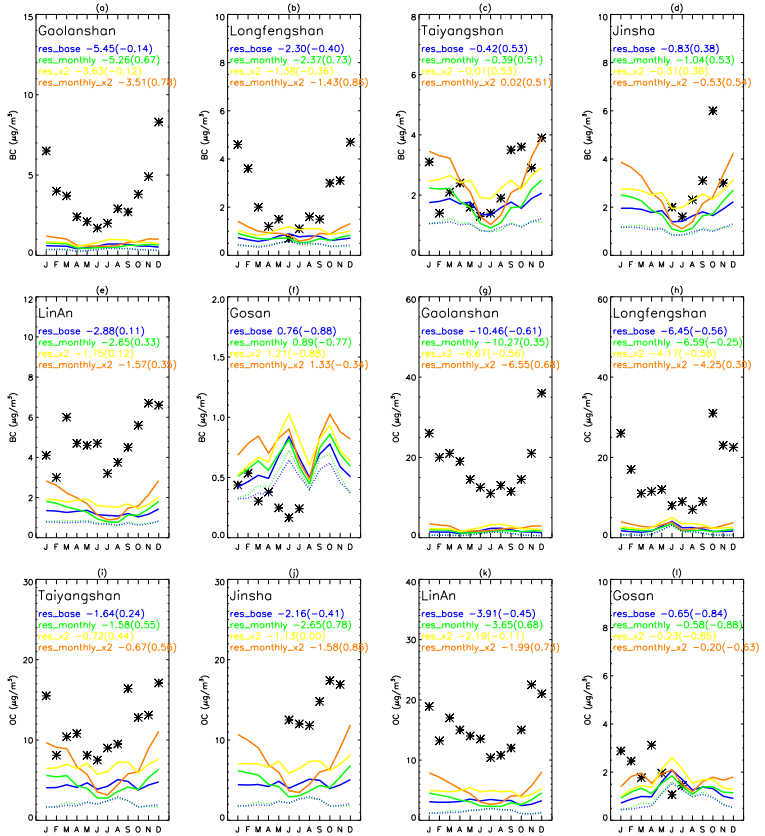

Figure 5. Observed (black stars) and simulated monthly mean BC **(a–f)** and OC **(g–l)** at East Asian locations. Normalised mean bias factor (NMBF) and correlation coefficient (r) are reported for each model simulation: NMBF(r). Experiments where residential emissions have been removed are represented by the blue (res_base_off) and green (res_monthly_off) dotted lines.

ACPD
15, 20449–20520, 2015

The impact of residential combustion emissions

E. W. Butt et al.

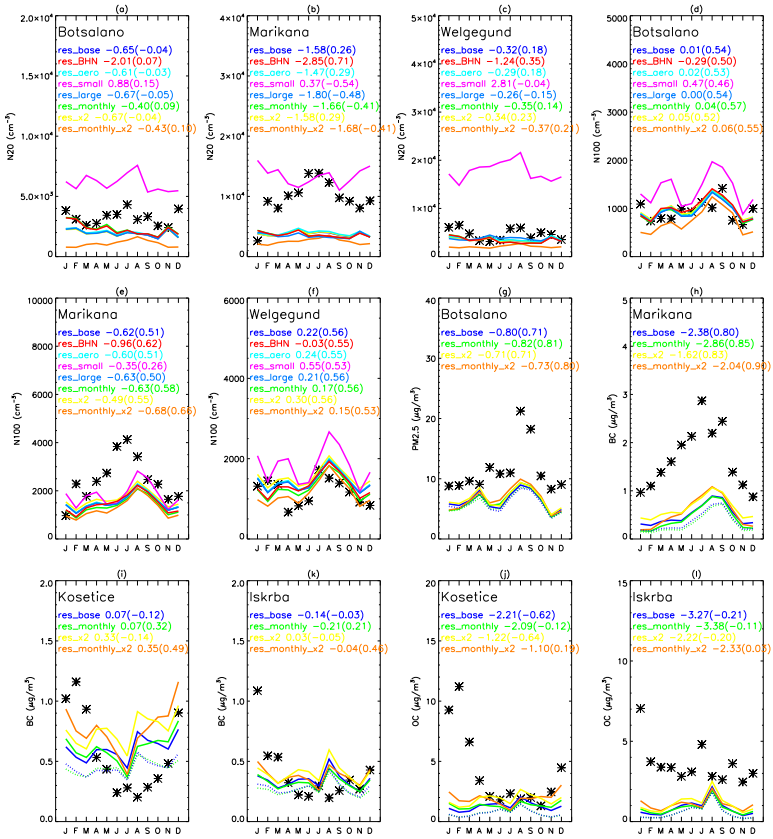

Figure 6. Observed (black stars) and simulated monthly mean N_{20} **(a–c)**, N_{100} **(d–f)**, $PM_{2.5}$ **(g)**, BC **(h–k)** and OC **(j–l)** at Southern African and Eastern European locations. Normalised mean bias factor (NMBF) and correlation coefficient (r) are reported for each model simulation: NMBF(r). Experiments where residential emissions have been removed are represented by the blue (res_base_off) and green (res_monthly_off) dotted lines.

ACPD
15, 20449–20520, 2015

The impact of residential combustion emissions

E. W. Butt et al.

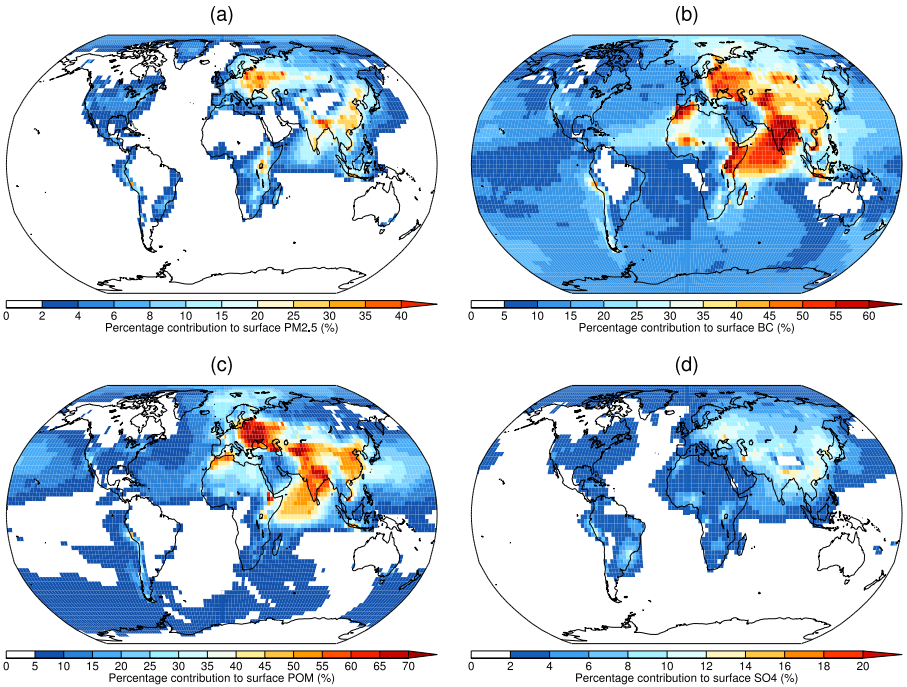

Figure 7. Percentage contribution of residential emissions to annual surface mean $PM_{2.5}$ **(a)**, BC **(b)**, POM **(c)** and sulfate (SO_4) **(d)** concentrations for the baseline simulation (res_base), relative to an equivalent simulation where residential emissions have been removed (res_base_off).

ACPD
15, 20449–20520, 2015

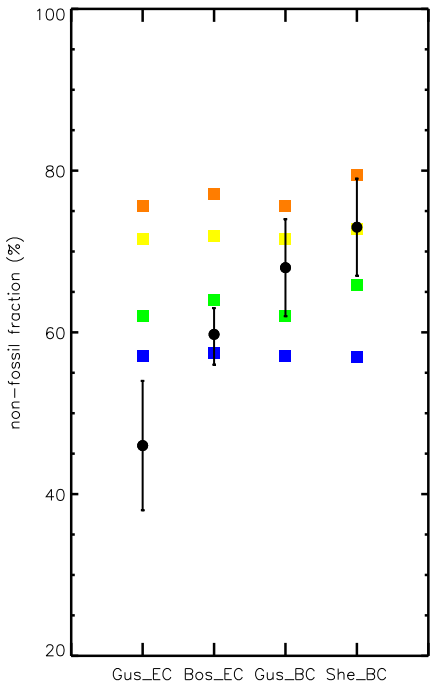

Figure 8. Comparison of simulated (squares) and observed (circles, error bars show uncertainty range) contribution of non-fossil (residential biofuel and open biomass burning) sources to BC concentrations at Hanimaadhoo, Indian Ocean. Observations are from Gustafsson et al. (2009) ("Gus EC" (thermo-optical) and "Gus BC" (optical) for January–March), Bosch et al. (2014) ("Bos EC" (thermo-optical) for February–March) and Sheesley et al. (2012) ("She BC" (optical) for November–February). Model simulations are represented by squares: standard emissions (blue: res base; green: res_monthly) and where residential carbonaceous emissions have been doubled (yellow: res_×2; orange: res_monthly_×2). Simulated fractional contributions are averaged over the time of year that the observations were made.

ACPD
15, 20449–20520, 2015

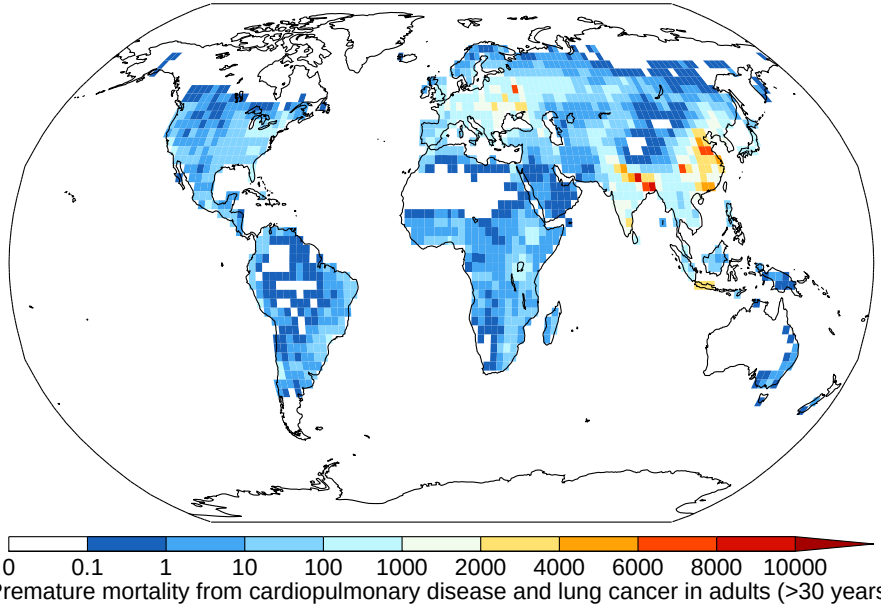

Figure 9. Simulated annual premature mortality (cardiopulmonary diseases and lung cancer) due to ambient exposure to ambient $PM_{2.5}$ from residential emissions (res_base).

ACPD
15, 20449–20520, 2015

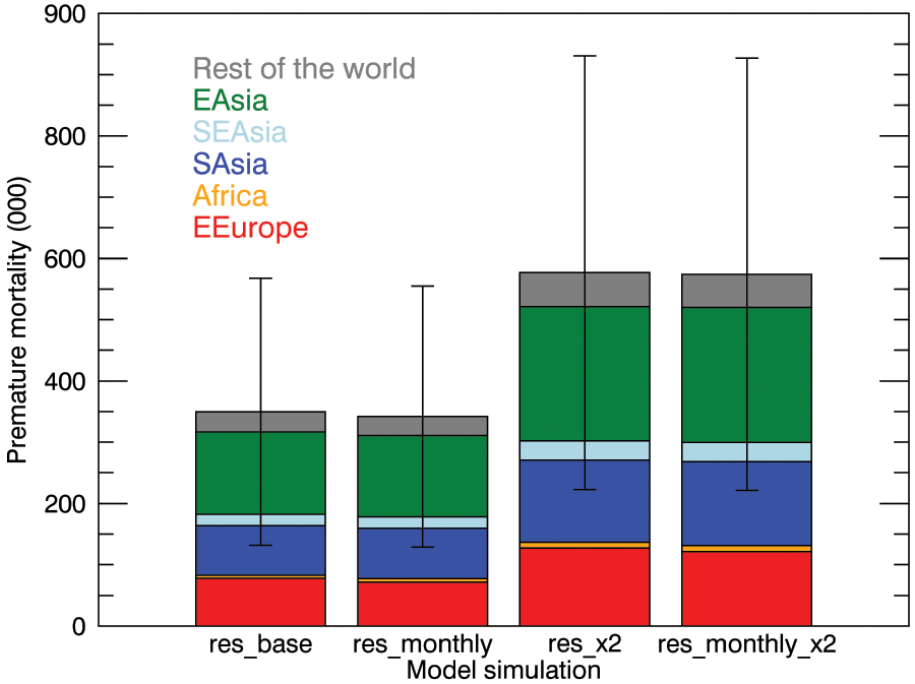

Figure 10. Simulated global annual premature mortality (cardiopulmonary diseases and lung cancer for persons over the age of 30 years) due to exposure to ambient $PM_{2.5}$ from residential emissions. Results are shown for standard emissions (res_base and res_monthly) and where residential emissions have been doubled (res_×2 and res_monthly_×2). Mortality is shown for Eastern Europe (EEurope), Africa (Africa), South Asia (SAsia), South East Asia (SEAsia), East Asia (EAsia) and rest of the world (as defined in Fig. 2).

ACPD
15, 20449–20520, 2015

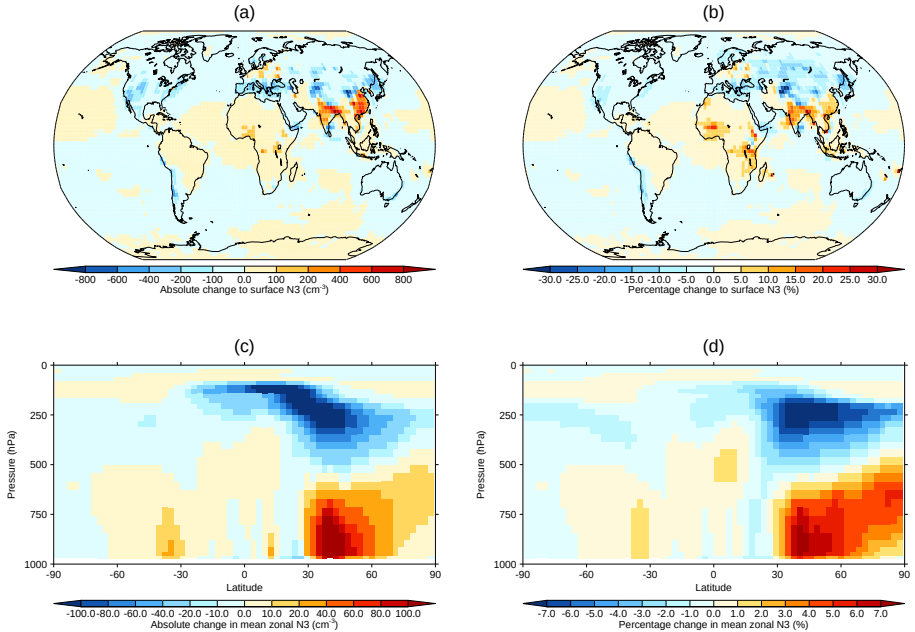

Figure 11. Simulated absolute and percentage change in annual mean surface **(a–b)** and zonal **(c–d)** number concentration (N_3; greater than 3 nm dry diameter) due to residential emissions (res_base), relative to an equivalent simulation where residential emissions have been removed (res_base_off).

ACPD
15, 20449–20520, 2015

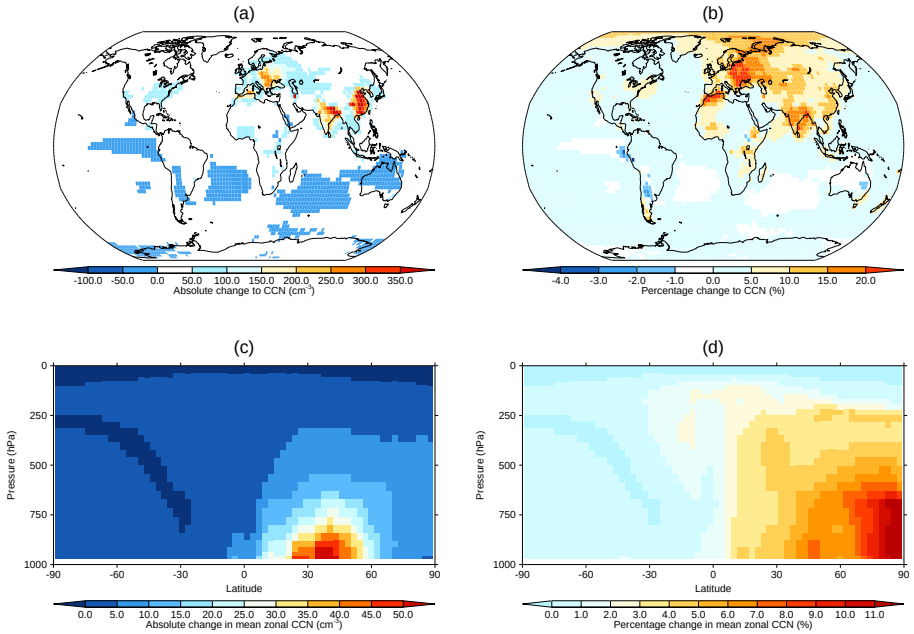

Figure 12. Simulated absolute and percentage change in annual mean surface **(a–b)** and zonal **(c–d)** CCN (N_{50}) concentrations due to residential emissions (res_base), relative to an equivalent simulation where residential emissions have been removed (res_base_off).

ACPD
15, 20449–20520, 2015

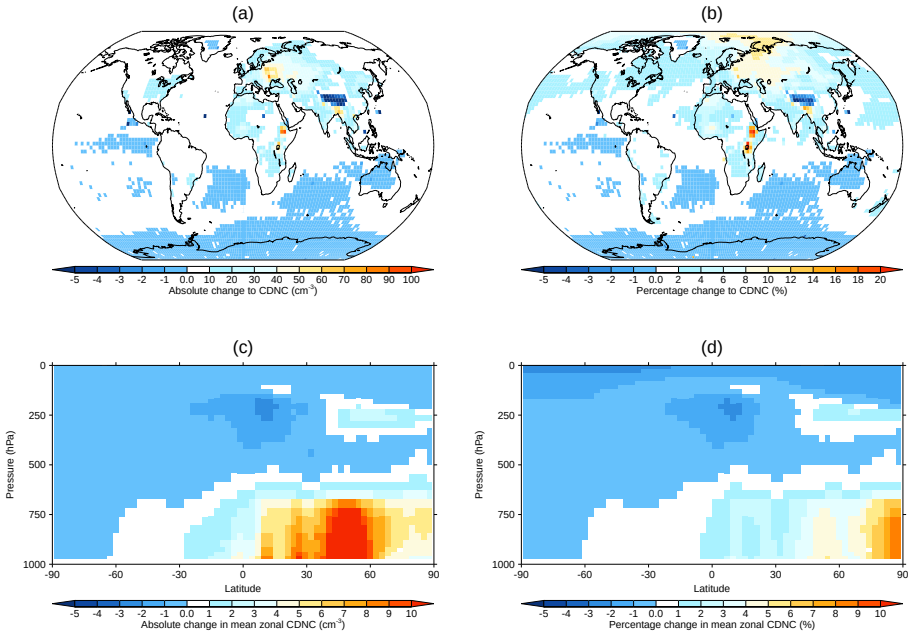

Figure 13. Simulated absolute and percentage change in annual mean at low cloud height (850–900 hPa) **(a–b)** and zonal **(c–d)** CDNC due to residential emissions (res_base), relative to an equivalent simulation where residential emissions have been removed (res_base_off).

ACPD
15, 20449–20520, 2015

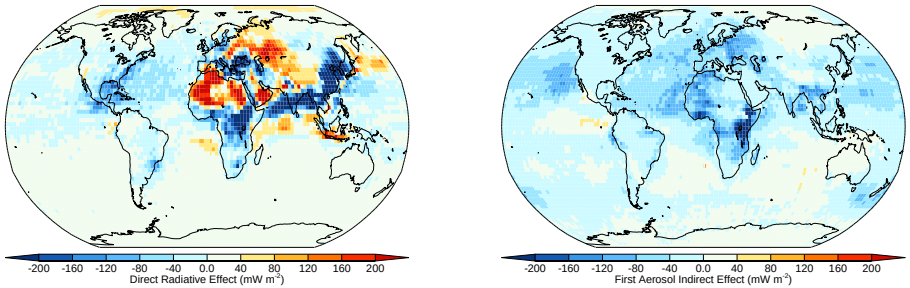

Figure 14. Annual mean all-sky direct radiative effect (DRE) (left), and first aerosol indirect effect (AIE) (right) due to residential emissions (res_base), relative to an equivalent simulation where residential emissions have been removed (res_base_off).

ACPD
15, 20449–20520, 2015

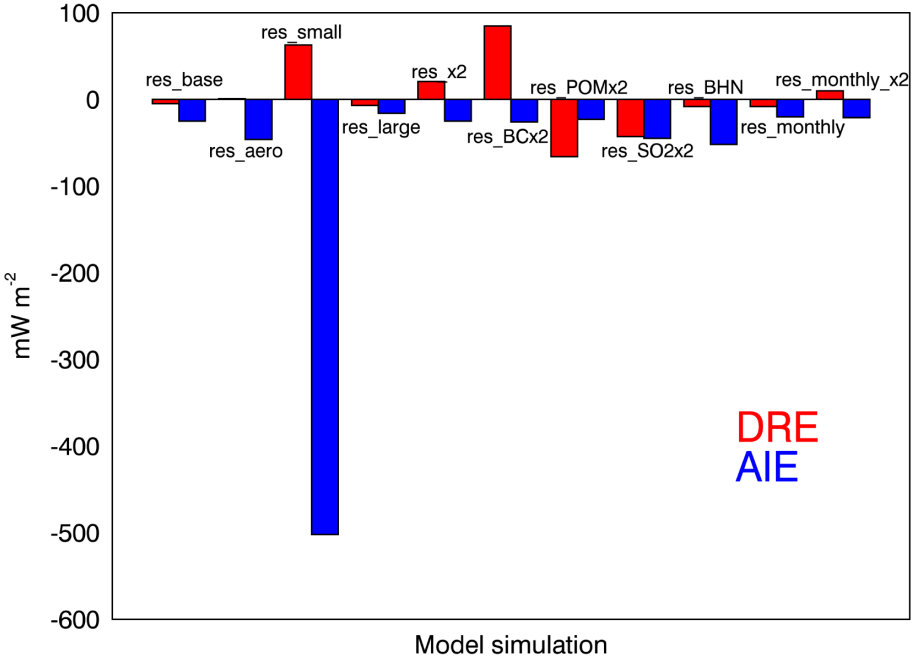

Figure 15. Global annual mean all-sky direct radiative effect (DRE) (red) and first aerosol indirect effect (AIE) (blue) for all model simulations due to the impact of residential combustion emission, relative to simulations where residential combustion emissions have been removed. DRE and AIE values for each simulation are detailed in Table 3.

ACPD
15, 20449–20520, 2015